J|A|C|S
ARTICLES
Published on Web 10/12/2002

X-ray Absorption and Resonance Raman Studies of Methyl-Coenzyme M Reductase Indicating That Ligand Exchange and Macrocycle Reduction Accompany Reductive Activation†

Qun Tang,‡ Paul E. Carrington,§ Yih-Chern Horng,|| Michael J. Maroney,*,§ Stephen W. Ragsdale,*,|| and David F. Bocian*,‡

Contribution from the Department of Chemistry, University of California, Riverside, California 92521-0403, Department of Chemistry, University of Massachusetts, Amherst, Massachusetts, and Department of Biochemistry, Beadle Center, University of Nebraska, Lincoln, Nebraska 68588-0664

Received February 28, 2002. Revised Manuscript Received August 13, 2002

Abstract: Methyl-coenzyme M reductase (MCR) catalyzes methane formation from methyl-coenzyme M (methyl-SCoM) and *N*-7-mercaptoheptanoylthreonine phosphate (CoBSH). MCR contains a nickel hydrocorphin cofactor at its active site, called cofactor F_{430}. Here we present evidence that the macrocyclic ligand participates in the redox chemistry involved in catalysis. The active form of MCR, the red1 state, is generated by reducing another spectroscopically distinct form called ox1 with titanium(III) citrate. Previous electron paramagnetic resonance (EPR) and ^{14}N electron nuclear double resonance (ENDOR) studies indicate that both the ox1 and red1 states are best described as formally Ni(I) species on the basis of the character of the orbital containing the spin in the two EPR-active species. Herein, X-ray absorption spectroscopic (XAS) and resonance Raman (RR) studies are reported for the inactive (EPR-silent) forms and the red1 and ox1 states of MCR. RR spectra are also reported for isolated cofactor F_{430} in the reduced, resting, and oxidized states; selected RR data are reported for the ^{15}N and ^{64}Ni isotopomers of the cofactor, both in the intact enzyme and in solution. Small Ni K-edge energy shifts indicate that minimal electron density changes occur at the Ni center during redox cycling of the enzyme. Titrations with Ti(III) indicate a 3-electron reduction of free cofactor F_{430} to generate a stable Ni(I) state and a 2-electron reduction of Ni(I)-ox1 to Ni(I)-red1. Analyses of the XANES and EXAFS data reveal that both the ox1 and red1 forms are best described as hexacoordinate and that the main difference between ox1 and red1 is the absence of an axial thiolate ligand in the red1 state. The RR data indicate that cofactor F_{430} undergoes a significant conformational change when it binds to MCR. Furthermore, the vibrational characteristics of the ox1 state and red1 states are significantly different, especially in hydrocorphin ring modes with appreciable C=N stretching character. It is proposed that these differences arise from a 2-electron reduction of the hydrocorphin ring upon conversion to the red1 form. Presumably, the ring-reduction and ligand-exchange reactions reported herein underlie the enhanced activity of MCR_{red1}, the only form of MCR that can react productively with the methyl group of methyl-SCoM.

I. Introduction

Methyl-coenzyme M reductase (MCR) catalyzes the final step in methane formation from methyl-coenzyme M (methyl-SCoM) and *N*-7-mercaptoheptanoylthreonine phosphate (CoBSH) (eq 1).[1]

$$\text{methyl-SCoM} + \text{CoBSH} \rightarrow \text{CH}_4 + \text{CoBS}-\text{SCoM} \quad (1)$$

CoBSH serves as the electron donor,[2] and the mixed disulfide CoBS−SCoM is the product of the oxidative half-reaction. At the active site of MCR is cofactor F_{430}, which is a nickel hydrocorphin.[3−5] The structure of cofactor F_{430} is shown in Figure 1. X-ray crystallographic studies of MCR reveal that

* Address correspondence to these authors. E-mail: David.Bocian@ucr.edu (D.F.B.); sragsdal1@unl.edu (S.W.R.); mmaroney@chemserv.chem.umass.edu (M.J.M.).

† Abbreviations used: MCR, methyl-coenzyme M reductase; methyl-SCoM, methyl-coenzyme M; CoBSH, *N*-7-mercaptoheptanoylthreonine phosphate or coenzyme B; CoBS−SCoM, the heterodisulfide product of the MCR reaction; EDC, 1-ethyl-3-(3-dimethylaminopropyl)carbodiimide hydrochloride; EPR, electron paramagnetic resonance; ENDOR, electron nuclear double resonance; sulfo-NHS, *N*-hydroxysulfosuccinimide; RR, resonance Raman; TBAH, tetrabutylammonium hexafluorophosphate; TAPS, (*N*-tris[hydroxymethyl]-3-aminopropanesulfonic acid ([2-hydroxy-1,1-bis-(hydroxymethyl)ethyl]amino)-1-propanesulfonic acid); XANES, X-ray Absorption near-edge structure; EXAFS, extended X-ray absorption fine structure; OEiBC, octaethylisobacteriochlorin.

‡ University of California.
§ University of Massachusetts.
|| University of Nebraska.

(1) DiMarco, A. A.; Bobik, T. A.; Wolfe, R. S. *Annu. Rev. Biochem.* **1990**, *59*, 355−394.
(2) Ellermann, J.; Kobelt, A.; Pfaltz, A.; Thauer, R. K. *FEBS Lett.* **1987**, *220*, 358−362.
(3) Diekert, G.; Klee, B.; Thauer, R. K. *Arch. Microbiol.* **1980**, *124*, 103−106.
(4) Diekert, G.; Jaenchen, R.; Thauer, R. K. *FEBS Lett.* **1980**, *119*, 118−120.
(5) Whitman, W. B.; Wolfe, R. S. *Biochem. Biophys. Res. Commun.* **1980**, *92*, 1196−1201.

10.1021/ja020314h CCC: $22.00

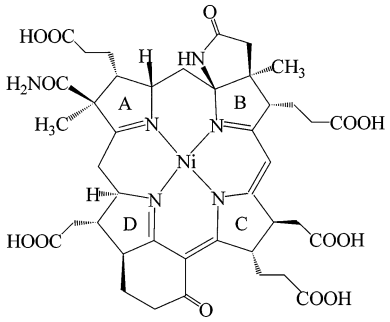

F_{430}

Figure 1. Structure of cofactor F_{430}.

Scheme 1. Scheme Describing the Various States of MCR Studied Here

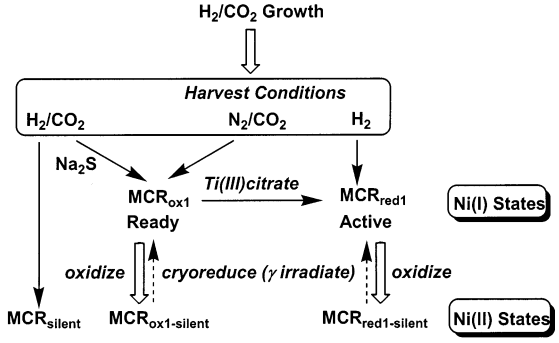

cofactor F_{430} forms the base of a narrow well that accommodates the two substrates and shields the reaction from solvent.[6] The phosphate group of CoBSH binds at the upper lip of the well with its thiol group located 6 Å from the central Ni atom of F_{430}.

The goal of the spectroscopic studies described herein is to characterize the Ni coordination and oxidation states of the catalytically important MCR_{ox1} and MCR_{red1} forms of the enzyme and to compare these states with the inactive Ni(II) forms of MCR and with the Ni(I), Ni(II), and Ni(III) states of cofactor F_{430} in solution. High-resolution crystal structures are available for the three EPR-silent and inactive Ni(II) states of the enzyme.[6−8] In the "MCR-silent" state, the Ni(II) ions in MCR are octahedral with four planar nitrogen atoms from the tetrapyrrole and a lower axial "proximal" ligand donated by the side-chain oxygen of Gln-α147. In MCR_{silent}, the exogenous, upper "distal" ligand is a sulfonate oxygen of CoBS−SCoM,[6] whereas, in the $MCR_{ox1\text{-}silent}$[6] and $MCR_{red1\text{-}silent}$[7] states, the thiol(ate) group of CoM−S(H) is the sixth ligand. CoM or methyl-SCoM binds as an upper axial nickel ligand in one of two conformations, depending on the state of the enzyme.

Scheme 1 summarizes the interrelationship among the different forms of MCR studied here and how these states are generated. All Ni(II) states are inactive, yet structurally characterized, and crystal structures of the important Ni(I) states are lacking because they are extremely labile. The MCR_{red1} form of the enzyme, which is a Ni(I) state, is required to initiate catalysis.[9−11] MCR_{red1} is formed by treating MCR_{ox1}, the "ready" state, with the low-potential reductant titanium(III) citrate.[11] The MCR_{red1} state also is generated, albeit in lower yield, when cells are bubbled with 100% H_2, before harvesting.[9] MCR_{ox1} is formed by replacing the H_2/CO_2 gas medium of growing cells with N_2/CO_2[9] *or* by adding sodium sulfide to the growth medium just before harvesting.[12] On the basis of the results of EPR and ENDOR studies, the ox1 and red1 states appear to contain Ni-(I).[13,14] Another proposed catalytically active state of MCR contains a methyl group, derived from methyl-SCoM, as the upper axial nickel ligand; it is this methyl group that is thought to undergo protonolysis to form methane.[15] The Ni(II) state, MCR_{silent}, is present when H_2/CO_2-grown cells are harvested without any special treatment. The Ni(I) ox1 and red1 states decay to form their designated Ni(II) states by a process that is accelerated by oxygen treatment.

Assuming that both the ox1 and red1 states contain Ni(I), what is the difference between the "ready" ox1 and the "active" red1 states? The XAS and RR spectroscopic studies reported here address this question. XAS is a sensitive probe of the coordination and oxidation states of metal ions. Prior XAS studies of cofactor F_{430} and MCR have shown that the isolated cofactor exists in solution as mixtures of low-spin four-coordinate and high-spin six-coordinate species.[16,17] The Ni(II) center in the cofactor adopts a six-coordinate geometry upon incorporation into the protein[16] to give MCR_{silent}. Conversion from low-spin four-coordinate Ni(II) to high-spin six-coordinate Ni(II) results in a lengthening of the Ni−N bond in the macrocycle from 1.9 to 2.1 Å. This increase in the Ni−N bond distance points to the flexibility of the F_{430} macrocycle, which was shown to be an important parameter in generating Ni(I) species upon reduction (as opposed to macrocycle radicals) in XAS studies of isolated F_{430} and nickel tetrapyrrole model compounds.[18−20] These studies concluded that the isolated cofactor in the Ni(I) state was in a distorted four-coordinate geometry.

RR spectroscopy is a sensitive probe of the conformation/axial-ligation state of tetrapyrrolic macrocycles.[21,22] RR studies have been previously used to examine both MCR and cofactor

(6) Ermler, U.; Grabarse, W.; Shima, S.; Goubeaud, M.; Thauer, R. K. *Science* **1997**, *278*, 1457−1462.
(7) Grabarse, W. G.; Mahlert, F.; Duin, E. C.; Goubeaud, M.; Shima, S.; Thauer, R. K.; Lamzin, V.; Ermler, U. *J. Mol. Biol.* **2001**, *309*, 315−330.
(8) Grabarse, W. G.; Mahlert, F.; Shima, S.; Thauer, R. K.; Ermler, U. *J. Mol. Biol.* **2000**, *303*, 329−344.
(9) Albracht, S. P. J.; Ankel-Fuchs, D.; Böcher, R.; Ellermann, J.; Moll, J.; van der Zwann, J. W.; Thauer, R. K. *Biochim. Biophys. Acta* **1988**, *941*, 86−102.
(10) Rospert, S.; Böcher, R.; Albracht, S. P. J.; Thauer, R. K. *FEBS Lett.* **1991**, *291*, 371−375.
(11) Goubeaud, M.; Schreiner, G.; Thauer, R. K. *Eur. J. Biochem.* **1997**, *243*, 110−114.
(12) Becker, D. F.; Ragsdale, S. W. *Biochemistry* **1998**, *37*, 2639−2647.
(13) Telser, J.; Davydov, R.; Horng, Y. C.; Ragsdale, S. W.; Hoffman, B. M. *J. Am. Chem. Soc.* **2001**, *123*, 5853−5860.
(14) Telser, J.; Horng, Y.-C.; Becker, D.; Hoffman, B.; Ragsdale, S. W. *J. Am. Chem. Soc.* **2000**, *122*, 182−183.
(15) Thauer, R. K. *Microbiology (Reading, U.K.)* **1998**, *144*, 2377−2406.
(16) Eidsness, M. K.; Sullivan, R. J.; Schwartz, J. R.; Hartzell, P. L.; Wolfe, R. S.; Flank, A. M.; Cramer, S. P.; Scott, R. A. *J. Am. Chem. Soc.* **1986**, *108*, 3120−3121.
(17) Shiemke, A. K.; Shelnutt, J. A.; Scott, R. A. *J. Biol. Chem.* **1989**, *264*, 11236−11245.
(18) Furenlid, L. R.; Renner, M. W.; Smith, K. M.; Fajer, J. *J. Am. Chem. Soc.* **1990**, *112*, 1634−1635.
(19) Furenlid, L. R.; Renner, M. W.; Fajer, J. *J. Am. Chem. Soc.* **1990**, *112*, 8987−8989.
(20) Renner, M. W.; Furenlid, L. R.; Barkigia, K. M.; Forman, A.; Shim, H. K.; Simpson, D. J.; Smith, K. M.; Fajer, J. *J. Am. Chem. Soc.* **1991**, *113*, 6891−6898.
(21) Spiro, T. G.; Li, X.-Y. In *Biological Applications of Raman Spectroscopy*; Spiro, T. G., Ed.; Wiley-Interscience: New York, 1988; Vol. III, pp 1−38.
(22) Procyk, A. D.; Bocian, D. F. *Annu. Rev. Phys. Chem.* **1992**, *43*, 465−496.

F_{430};[17,23−26] however, these RR studies examined only MCR_{silent} and Ni(II)F_{430}. To date, there have been no reported RR studies performed on MCR_{red1}, MCR_{ox1}, or the Ni(I) (or Ni(III)) complexes of cofactor F_{430}. Such studies have the potential for providing new insights into conformation/axial-ligation state(s) of the active site of MCR. For example, the macrocyclic ring structure of cofactor F_{430} in solution exhibits substantial deviation from planarity in the Ni(I) state, which is four-coordinate,[19] but it is not clear how flexible the ring is in the enzyme-bound cofactor.

Herein, we report XAS and RR studies of MCR in the EPR-silent Ni(II) and in the EPR-active MCR_{red1} and MCR_{ox1} states. XAS is used to examine Ni-centered redox chemistry and changes in axial ligation that accompany the redox process. RR spectroscopy is employed to probe changes in the structure of the F_{430} macrocycle that result from the redox chemistry. The XAS studies confirm that the ox1 and red1 states contain the same formal oxidation state of Ni and that both are more reduced than the EPR-silent Ni(II) state, consistent with the Ni(I) formalism for the EPR-active species. XANES analysis shows that the cofactor is always six-coordinate, and EXAFS analysis indicates that the difference between the ox1 and red1 states is reflected in part by a change of one axial ligand from a S donor to an O/N donor. These results imply an important role for the macrocycle in the reductive conversion of ox1 to red1. These changes are addressed using RR spectroscopy. To provide insight into how the protein affects the structure of cofactor F_{430}, we also have examined the RR spectra of isolated cofactor F_{430} in the Ni(I) and Ni(III) oxidation states. The RR spectra of MCR_{silent} and Ni(II)F_{430} were also reexamined to provide benchmarks for the studies of the other enzyme and cofactor species. The RR studies of both the enzyme and isolated cofactor are augmented with investigations of ^{15}N and ^{64}Ni isotopomers. The RR spectroscopic results show that cofactor F_{430} undergoes a significant conformational change when it binds to MCR. Conversion from MCR_{ox1} to MCR_{red1} involves major conformational rearrangements, which we propose are due to a 2-electron reversible reduction of the hydrocorphin ring of F_{430}. These changes occur in addition to an axial ligand "switch" in which the upper axial thiolate ligand is replaced by a N/O donor ligand. Presumably, these changes trigger the activation to a state (MCR_{red1}) that can react productively with the methyl group of methyl-SCoM.

II. Experimental Section

A. Biochemistry. 1. Materials. $^{15}NH_4Cl$ was obtained from Cambridge Isotope Laboratories. $^{64}NiCl_2$ was prepared by dissolving 10 mg (0.164 mmol) of elemental ^{61}Ni (93.4% purity, Pennwood Chemical) in 2 mL of 30% (v/v) HCl. Methylamine hydrochloride was obtained from Aldrich. *N*-Hydroxysulfosuccinimide (sulfo-NHS) was obtained from Pierce Chemical. 1-Ethyl-3-(3-dimethylaminopropyl)carbodiimide (EDC) hydrochloride was obtained from Sigma. Anhydrous acetonitrile was obtained from Fischer Scientific. These materials were used without further purification. Tetrabutylammonium hexafluorophosphate (TBAH) was obtained from Aldrich. TBAH was recrystallized three times from methanol and dried under vacuum at 110 °C. All other routine chemicals were obtained from Sigma.

2. Preparation of Enzyme and Growth Conditions. All manipulations of the enzyme were performed in a model PC-1-SSG anaerobic chamber (Vacuum Atmospheres Co., Hawthorne, CA) maintained below 1 ppm oxygen. The chamber is equipped with a UV−vis spectrometer (Ocean Optics, Dunedin, FL). Media were prepared as previously described.[27] MCR_{silent} and MCR_{ox1} were purified from *Methanothermobacter marburgensis*[28] as described earlier.[11,12,29] After purification, MCR was concentrated under argon (passed through an Oxisorb column) pressure in a 10 mL omegacell (Filtron) with a 30 kDa molecular mass cutoff. MCR_{red1} was prepared by activation of MCR_{ox1} with titanium(III) citrate.[11] The purity of the MCR_{ox1} and MCR_{red1} samples was assessed by EPR spectroscopy on a Bruker ESP 300E spectrometer equipped with an Oxford ITC4 temperature controller, a Hewlett-Packard model 5340 automatic frequency counter, and a Bruker gaussmeter. Double integrations of the EPR spectra were performed with copper perchlorate (1 mM) as the standard. Typical experimental conditions are temperature 100 K, microwave power 10 mW, microwave frequency 9.43 GHz, receiver gain 2×10^4, modulation amplitude 12.8 G, and modulation frequency 100 kHz. $MCR_{ox1\text{-}silent}$ was prepared by exposing MCR_{ox1} to air in 50 mM Tris−HCl, pH 7.6, at room temperature for 3−4 days, which decreases the spin intensity to below 0.01 spin/mol. This method is similar to that used in preparing the ox1-silent enzyme for crystallization studies.[6] Protein concentrations were determined by the Bradford method (Bio-Rad, Inc., reagent) with bovine serum albumin as a standard.[30] The F_{430} content was estimated using an extinction coefficient of 22000 M^{-1} cm^{-1} at 420 nm.[31] MCR assays were performed at 65 °C as described.[12]

3. Preparation of Ni(I)-, Ni(II)-, and Ni(III)F_{430}. Ni(II)F_{430} samples were prepared from purified MCR. Typically, MCR was treated with 30% (v/v) HCl(aq) to a pH below 1.0, resulting in precipitation of the protein and release of cofactor F_{430} into solution. After centrifugation, NaOH was added to the supernatant to adjust the pH to 7.0. This solution was desalted 3−4 times, and concentrated using an Amicon ultrafiltration cell with a 0.5 kDa molecular mass cutoff at 4 °C. After lyophilization, purified Ni(II)F_{430} was dissolved in anaerobic water.

Ni(I)F_{430} was prepared chemically, by reducing Ni(II)F_{430} with titanium(III) citrate at pH 10.0.[32] The formation of the reduced species was confirmed by absorption spectroscopy.

Ni(III)F_{430} was obtained via electrochemical oxidation of the pentamethylamide derivative of cofactor F_{430}. The pentamethylamide was used because bulk oxidation cannot be performed in an aqueous medium, and the native (pentaacid) form of cofactor F_{430} is insoluble in the organic solvents required for electrolysis. The methylamide derivative was prepared from the native cofactor as previously described.[33] Following this procedure, we were unable to obtain complete conversion to the desired pentamethyl derivative. The pentamethyl derivative was isolated from the mixture containing incompletely amidated cofactor by reversed-phase chromatography with a 10 mm × 250 mm Vydac column using aqueous trifluoroacetic acid (TFA) as the solvent. The identity of the pentamethylamide was confirmed via mass spectrometry (Voyager-DE, Perceptive Biosystems).

The bulk electrolysis was carried out in a three-compartment electrochemical cell (Pt wire working electrode, Pt mesh counter

(23) Shiemke, A. K.; Kaplan, W. A.; Hamilton, C. L.; Shelnutt, J. A.; Scott, R. A. *J. Biol. Chem.* **1989**, *264*, 7276−7284.
(24) Shiemke, A. K.; Eirich, L. D.; Loehr, T. M. *Biochim. Biophys. Acta* **1983**, *748*, 143−147.
(25) Shiemke, A. K.; Shelnutt, J. A.; Scott, R. A. *J. Am. Chem. Soc.* **1988**, *110*, 1645−1646.
(26) Li, M. Ph.D. Thesis, University of Georgia, Athens, GA, 1993.
(27) Schönheit, P.; Moll, J.; Thauer, R. K. *Arch. Microbiol.* **1980**, *127*, 59−65.
(28) Wasserfallen, A.; Nolling, J.; Pfister, P.; Reeve, J.; Conway de Macario, E. *Int. J. Syst. Evol. Microbiol.* **2000**, *50 Pt 1*, 43−53.
(29) Horng, Y.-C.; Becker, D. F.; Ragsdale, S. W. *Biochemistry* **2001**, *40*, 12875−12885.
(30) Bradford, M. M. *Anal. Biochem.* **1976**, *72*, 248−254.
(31) Pfaltz, A.; Juan, B.; Fassler, A.; Eschenmoser, A.; Jaenchen, R.; Gilles, H. H.; Diekert, G.; Thauer, R. K. *Helv. Chim. Acta* **1982**, *65*, 828−865.
(32) Holliger, C.; Pierik, A. J.; Reijerse, E. J.; Hagen, W. R. *J. Am. Chem. Soc.* **1993**, *115*, 5651−5656.
(33) Hamilton, C. L.; Ma, L.; Renner, M. W.; Scott, R. A. *Biochim. Biophys. Acta* **1991**, *1074*, 312−319.

electrode, Ag/Ag^+ (butyronitrile) reference electrode) at a potential of 0.93 V using standard instrumentation (PAR 175 universal programmer and PAR 173 potentiostat). This potential is ~90 mV above the measured $E_{1/2}$ value for the pentamethylamide (~0.84 V; ferrocene/ferrocenium, $E_{1/2} = 0.02$ V). The solvent was acetonitrile containing 0.1 M TBAH as the supporting electrolyte. The bulk electrolysis was conducted with the electrochemical cell initially housed in a glovebox (Vacuum Atmospheres HE-93). The formation of the Ni(III) complex was confirmed by transferring a small amount of sample to an optical cuvette, which was then tightly sealed, removed from the glovebox, and examined via absorption spectroscopy. The electrochemical cell was then removed from the glovebox and transferred to the Raman instrument where the potential was reestablished at 0.93 V and maintained there for the duration of the Raman experiment (vide infra).

4. Redox Titration of MCR and Coenzyme F_{430} with Titanium(III) Citrate. Redox titrations of MCR were performed by incubating 80 μM MCR_{ox1} (0.49 spin/mol) at 60 °C with varying concentrations of titanium(III) citrate for 30 min in 1 M TAPS buffer, pH 10.0. The conversion to MCR_{red1} was measured by EPR spectroscopy, performed as described above. The data were fit with the sigmoidal equation $f = a/(1 + \exp(-(x - x_0)/b))$. The amount of Ti(III) present in solution was determined by EPR spectroscopy and by titrating standardized solutions of methyl viologen.

Titrations of F_{430} were performed in the anaerobic chamber at pH values of 7.6 and 10.0. Varying amounts of a standardized Ti(III) solution were added to a solution of F_{430}, and samples were removed for UV−vis and EPR spectroscopy. A 0.7 mL aliquot was monitored by UV−vis spectroscopy to measure the concentrations of Ni(I)- and Ni(II)F_{430}, and a 0.2 aliquot was added to an EPR tube and was immediately frozen for EPR determination of the concentrations of Ni(I)F_{430} and Ti(III) after the UV−vis spectrum was stable.

B. Spectroscopy. 1. XAS Data Collection and Analysis. Four states of MCR were examined using XAS: MCR_{silent}, $MCR_{ox1\text{-}silent}$, MCR_{ox1}, and MCR_{red1}. The samples of MCR_{silent} and $MCR_{ox1\text{-}silent}$ appear to be homogeneous; however, the samples of MCR_{ox1} and MCR_{red1} were only partially poised in those states. EPR analysis reveals that, while the only EPR-active species in each sample is the one designated, the spin quantitation vs Ni concentration in the sample ranged from 0.57 to 0.63. Because the samples are mixtures where the major component is the state of interest (the remainder is likely to be the corresponding EPR-silent state), the XAS spectra obtained are weighted averages of at least two species.

Data collection for each of the XAS samples was conducted over several sessions using beam line X9B at the National Synchrotron Light Source (NSLS) at Brookhaven National Laboratories. The samples were contained in polycarbonate holders that were inserted into a slotted aluminum holder and held near 50 K using a He displex cryostat. Data were collected under dedicated conditions at 2.8 GeV and 160−260 mA as previously described,[34] except that a sagitally focusing Si(111) double-crystal monochromator was used for these studies. The X-ray energy of the focused monochromatic beam was internally calibrated to the first inflection point of Ni foil (8331.6 eV). Harmonic rejection was achieved by use of a Ni mirror.

XANES data were collected over the range from ca. 8100 to ca. 8500 eV, with the vertical primary aperture reduced to 0.3 mm. This arrangement gives a theoretical energy resolution of ca. 3 eV, and a spectral resolution comparable to that obtained on model compounds using a flat Si(220) double-crystal monochromator at this beam line, as previously described.[34] The spectral features are reproducible to within 0.1 eV in sequential scans.

EXAFS data for all four samples were collected over a scan range from 8100 to 9400 eV under the same conditions used for collection of XANES data, except that the vertical primary aperture was set at 1.0 mm. This arrangement results in lower energy resolution (ca. 5 eV), but provides higher X-ray beam intensity.

Table 1. XANES Analysis[a]

MCR species	Ni K-edge energy (eV)	1s → 3d peak area (10^2 eV)	MCR species	Ni K-edge energy (eV)	1s → 3d peak area (10^2 eV)
MCR_{silent}	8342.9(2)	3.2(3)	MCR_{ox1}	8342.5(1)	2.2(3)
$MCR_{ox1\text{-}silent}$	8343.0(1)	1.6(6)	MCR_{red1}	8342.4(1)	2.4(4)

[a] The Ni K-edge energy (E_k) for each sample is taken as the energy at the peak of the first derivative of the XANES region.

X-ray fluorescence data were collected using a 13-element Ge detector (Canberra). The integrity of the samples during ~10 h of exposure to monochromatic synchrotron radiation was determined by monitoring the Ni K-edge energy on sequential scans. No changes in either edge energy (redox state) or pre- or postedge XANES spectra (ligand environment) were observed. For the MCR_{ox1} and MCR_{red1} samples, EPR spectra obtained before and after exposure showed that no change in the EPR signal occurred as a result of exposure except for the production of solvated electrons. Samples were assayed for activity before and after exposure, and no significant decrease in activity was observed.

The XANES data reported are the average of three scans for each sample. EXAFS spectra reported are the sum of 6−12 scans and were analyzed in analogy with previously published procedures.[35] The data reported for MCR_{ox1} and MCR_{red1} represent the samples with the best spin quantitation available (~0.6 spin/Ni). For comparison, the Ni K-edge energy of the samples was taken to be the maximum of a Gaussian peak fitted to the first derivative of the Ni K-edge (inflection point). The edge energies shown in Table 1 represent the average of three fits using different data ranges, with their standard deviation. Because the MCR_{ox1} and MCR_{red1} samples are mixtures, the edge energies represent a weighted average of the species present in the sample and should be regarded as trends rather than absolute numbers. The peaks in preedge XANES spectra at ca. 8332 eV are assigned to 1s → 3d electronic transitions. The areas of these peaks were determined by fitting a baseline to the region of the normalized spectrum immediately below and above this feature in energy and integrating the difference.[36]

The EXAFS data were analyzed using WinXAS.[37] The summed, energy-calibrated data files were background-corrected and normalized using a two-polynomial fit, with a first-order polynomial for the preedge region and a third-order polynomial for the postedge region. The data were converted to k-space using the relationship $[2m_e(E - E_0)/\hbar^2]^{1/2}$ (where m_e is the electron mass, E is the photon energy, $\hbar$ is Planck's constant divided by 2π, and E_0 is the threshold energy of the absorption edge defined here as 8340.0 eV). A least-squares fitting procedure was employed over a k range of 2−12.5 Å^{-1} using Fourier-filtered EXAFS with a back-transform window of 1.1−3.3 Å (uncorrected for phase shifts). The presence of trace amounts of Cu in the samples required the data be truncated at $k = 12.5$ Å^{-1}. The fitting procedure minimized $\text{GOF} = 1/\sigma^2 \sum_{i=1}^{N} [y_{\text{exptl}}(i) - y_{\text{theor}}(i)]^2$ (where σ is an estimate of the experimental error, y_{exptl} and y_{theor} are experimental and theoretical data points, respectively, and N is the number of data points).[37] Comparison of residual values[37] (eq 2) and the difference in the disorder parameters between theoretical data and the fit, $|\sigma^2| = |(\sigma_{\text{fit}}^2 - \sigma_{\text{theor}}^2)|$, using the EXAFS formula (eq 3),[37] were used to select best fits of the data. The disorder parameter σ_{model}^2 was obtained from FEFF 6 calculations of crystallographically characterized models as described below.

(34) Bagyinka, C.; Whitehead, J. P.; Maroney, M. J. *J. Am. Chem. Soc.* **1993**, *115*, 3576−3585.

(35) Davidson, G.; Clugston, S. L.; Honek, J. F.; Maroney, M. J. *Biochemistry* **2001**, *40*, 4569−4582.

(36) Colpas, G. J.; Maroney, M. J.; Bagyinka, C.; Kumar, M.; Willis, W. S.; Suib, S. L.; Mascharak, P. K.; Baidya, N. *Inorg. Chem.* **1991**, *30*, 920−928.

(37) Ressler, T. *J. Phys. IV* **1997**, *7*, C2−269.

$$\text{residual [\%]} = \frac{\sum_{i=1}^{N} |y_{\text{exptl}}(i) - y_{\text{theor}}(i)|}{\sum_{i=1}^{N} |y_{\text{exptl}}(i)|} \times 100 \qquad (2)$$

$$\chi(k) = \sum_{j} \frac{N_j S_0^2 F_j(k)}{kR_j^2} e^{(-2k^2\sigma j^2)} e^{(-2Rj/\lambda)} \sin[2kR_j + \delta_j(k)] \qquad (3)$$

Initial fits of the EXAFS data from crystallographically characterized states of MCR (silent and ox1-silent) indicated that it was necessary to fit features arising from the F_{430} C atoms in the second coordination sphere of Ni to reliably detect and accurately fit data from axial ligands, particularly S donors at a distance of 2.3−2.4 Å (vide infra). To do this, FEFF 6[38−40] was used to calculate values for phases, amplitudes, and σ^2 for atoms in a model of the F_{430} macrocycle (Figure 2a) using the crystal structure of the $MCR_{ox1\text{-}silent}$ (Protein Data Bank file 1mro.pdb).[6] Photoelectron scattering pathways for all atoms in F_{430} were calculated out to a radial distance of 6.1 Å from the Ni ion (Figure 1). Because of the low symmetry of the F_{430} macrocycle (Figure 1), three single-scattering pathways were obtained from FEFF 6 calculations that accounted for the four Ni−N vectors (one shell of two N atoms, and two shells each of one N atom). To minimize the number of adjustable parameters, the Ni−N distance, *r*, and the σ^2 parameters for the three pathways were analyzed as a single correlated shell, separate from the axial N/O or S ligands that are also in the first coordination sphere of the Ni atom.

Parameters for single-scattering and multiple-scattering pathways involving eight C atoms in the second coordination sphere of the cofactor were also obtained from the FEFF 6 calculation. The calculation yields 91 pathways involving second coordination sphere C atoms. In analogy with our procedure developed for fitting all five non-hydrogen atoms of an imidazole ring,[35] only those scattering pathways with a relative intensity >15% were used in the data analysis to limit the number of free running parameters used in the fits. This resulted in the use of eight single-scattering and eight multiple-scattering pathways with four or fewer legs to model the EXAFS arising from the second coordination sphere C atoms in the cofactor. To further limit the number of adjustable parameters, the second coordination sphere C atoms were separated into three groups (one shell of four C atoms and two shells each of two C atoms), on the basis of similarities in the Ni−C distances in the $MCR_{ox1\text{-}silent}$ crystal structure, similarities in the phase shift parameters (E_0) from the FEFF 6 calculation, and empirical observations in initial fits of the data. The average Ni−C distance for each group was refined. The distances of multiple-scattering paths for a given shell were further constrained to be correlated to the distances of the constituent single-scattering paths. A single value of σ^2 was used to describe disorder for all eight C atoms. This resulted in four adjustable parameters (three distances, *r*, and one value of σ^2) for modeling the EXAFS arising from second coordination sphere C atoms. Thus, six adjustable parameters were used to fit EXAFS data arising from F_{430} (*r* and σ^2 for Ni−N; three *r* values and one σ^2 value for the eight second coordination sphere C atoms).

The FEFF 6 calculations also provided 109 single- and multiple-scattering pathways for the 12 C atoms in the third coordination sphere of Ni in F_{430}. Inclusion of these scattering atoms in our model for F_{430} EXAFS would have resulted in the number of free-running parameters (N_{frp}) in the fits greatly exceeding the number of independently determined parameters (N_{idp})/2 in the data sets ($N_{\text{idp}} = 17$). Because of this, and because EXAFS arising from third coordination sphere atoms does not interfere with the analysis of EXAFS arising from atoms in the first coordination sphere, the model for F_{430} was limited to the four N atoms in the first coordination sphere and the eight C atoms in the second coordination sphere (Figure 2b).

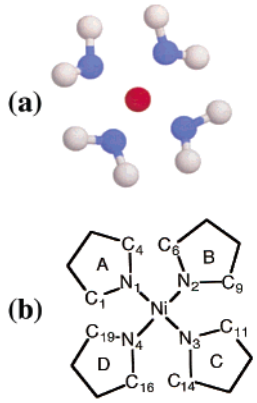

Figure 2. Truncated structure of F_{430} used in XAS analysis: (a) F_{430} atoms used in FEFF 6 calculations; (c) F_{430} atoms used to fit the EXAFS data.

For axial ligands, theoretical phases and amplitudes for single-scattering EXAFS analyses were obtained from FEFF 6 calculations of the crystal structures of structurally characterized model compounds, as previously described.[41,42] Photoelectron scattering pathways for the model compounds $[Ni(Im)_6](BF_4)_2$[43] and tetraethylammonium tetrakis-(*p*-chlorobenzenethiolato)nickelate(II), $(Et_4N)_2[Ni(p\text{-}SPhCl)_4]$,[44] were used to obtain single-scattering theoretical phase, amplitude, σ^2, and E_0 parameters for N and S, respectively. These parameters were tested by using them to fit experimentally obtained EXAFS data from the compounds whose structures were used in the calculations by varying only *r* and σ^2. Values obtained for *r* in this manner were in agreement with crystallographic values within 0.02 Å. Thus, each unique axial donor atom added two more adjustable parameters to the fits of MCR data, for a total of 8−10 free-running parameters used in fits to determine the axial ligation of cofactor F_{430} in MCR.

Fourier-filtered EXAFS data, using a back-transform window of 1.1−3.3 Å (uncorrected for phase shifts) that was designed to filter out contributions to the EXAFS from atoms beyond the second coordination sphere, were fit using our previously described restricted fit protocol, where values of *N* are held to integer values for each shell and not independently refined. Values of E_0 for each absorber−scatterer interaction were determined by FEFF 6 and not refined. In the case of a shell containing several atoms (i.e., groups of second coordination sphere C atoms) an average value of E_0 was determined and used for the shell. This eliminates the correlation between *N* and σ^2, and *r* and E_0, that occurs when all of these parameters are refined.

The following strategy was used to generate models that account for the EXAFS features arising from the Ni center in MCR samples: (i) The best single-shell fit to the data was determined by using four, five, or six O/N (*N* parameters from the F_{430} FEFF 6 calculation were used) or S donor atoms. While these fits were inadequate to describe the EXAFS of F_{430}, the residuals obtained from the fits provide a useful reference for further refinements of the data. (ii) Parameters describing EXAFS arising from the four first coordination sphere N atoms and eight second coordination sphere C atoms of F_{430} were used to obtain a fit to the data. (iii) To this fit were added all combinations of O/N or S scattering atoms, totaling one or two axial ligands.

(38) Mustre de Leon, J.; Rehr, J. J.; Zabinsky, S. I.; Albers, R. C. *Phys. Rev.* **1990**, *B44*, 4146−4156.
(39) Rehr, J. J.; Albers, R. C. *Phys. Rev.* **1990**, *B41*, 839−8149.
(40) Rehr, J. J.; Zabinsky, S. I.; Albers, R. C. *Phys. Rev. Lett.* **1992**, *69*, 3397−3400.
(41) Davidson, G.; Clugson, S. L.; Honek, J. F.; Maroney, M. J. *Inorg. Chem.* **2000**, *39*, 2962−2963.
(42) Davidson, G.; Choudhury, S. B.; Gu, Z. J.; Bose, K.; Roseboom, W.; Albracht, S. P. J.; Maroney, M. J. *Biochemistry* **2000**, *39*, 7468−7479.
(43) van Ingen Schenau, A. D. *Acta Crystallogr.* **1975**, *14*, 888−891.
(44) Rosenfield, S. G.; Armstrong, W. H.; Mascharak, P. K. *Inorg. Chem.* **1986**, *25*, 3014−3018.

Because the samples of MCR_{ox1} and MCR_{red1} are mixtures of EPR-active and -silent species, difference spectra resulting from the subtraction of MCR_{silent} and $MCR_{ox1\text{-}silent}$ were analyzed. To generate the difference spectra, the normalized spectrum of the EPR-silent species was multiplied by the amount determined to be present in the sample by EPR (35% or 37%) and subtracted from the normalized MCR_{silent} or $MCR_{ox1\text{-}silent}$ data, and the result renormalized. The resulting normalized difference spectrum was analyzed as before. In general, the results of these fits were comparable to those obtained on the uncorrected data. Because the identity of the EPR-silent species present in MCR_{ox1} and MCR_{red1} is not known, the results from uncorrected data are presented. Fits generated from the difference spectra may be found in the Supporting Information (Tables S2−S4).

2. RR Spectroscopy. The RR measurements on the MCR_{silent}, MCR_{red1}, MCR_{ox1}, Ni(II)F_{430}, and Ni(I)F_{430} samples were made on samples contained in tightly sealed 1 mm i.d. capillary tubes; the measurements on Ni(III)F_{430} were made on the sample housed in the sealed electrochemical cell. The working electrode compartment of the electrochemical cell is made from optical-quality quartz to optimize the quality of the RR measurements. The RR studies for the MCR, Ni(II)F_{430}, and Ni(I)F_{430} samples were made at a variety of temperatures ranging from cryogenic to ambient. For the cryogenic studies, the capillary tubes were mounted directly onto the cold tip of a closed-cycle liquid He refrigeration system (ADP Cryogenics DE-202). The RR measurements on the Ni(III)F_{430} sample were made only at ambient temperature.

The RR spectra were acquired with a triple spectrograph (Spex 1877) equipped with a holographically etched 2400 grooves/mm grating in the third stage. The excitation wavelengths were provided by the discrete outputs of a krypton ion (Coherent Innova 200-K3) or an argon ion (Coherent Innova 400-15 UV) laser. The scattered light was collected in a 90° configuration using a 50 mm f/1.4 Canon camera lens. A UV-enhanced charge-coupled device (CCD) was used as the detector (Princeton Instruments LN/CCD equipped with an EEV1152-UV chip). The data acquisition time for a typical spectrum was ∼3 h (90 × 120 s scans). Cosmic spikes were removed prior to addition of the data sets. The laser power at the sample was ∼7.5 mW. The spectral resolution was ∼2 cm^{-1}. The frequencies were calibrated using the known frequencies of indene and fenchone.

III. Results

A. Reductive Titration of MCRox1. MCR_{ox1} was titrated with varying amounts of Ti(III) in attempts to determine the number of electrons required to form MCR_{red1} (Figure 3A). The results indicate that 3 equiv of Ti(III) is required per mole of MCR_{red1} formed. In the absence of Ti(III), the 60 °C incubation at pH 10.0 results in nearly complete conversion of ox1 to an EPR-silent state. It is puzzling why the strong reductant titanium(III) citrate is required to effect the conversion of MCR_{ox1} to MCR_{red1}, given that both contain a Ni(I) ion. It seemed possible that the conversion actually is not a reductive activation and that some component of the reaction mixture might be responsible for the conversion, perhaps through a ligand-exchange or proton-transfer reaction. We determined requirements for the conversion by individually omitting one component of the reaction mixture (bicarbonate, citrate, Ti(III)) and found that only Ti(III) is absolutely required for the conversion. Ti(III) is thiophilic, so we considered that another thiophilic metal might be a suitable replacement. However, when zinc(II) citrate or titanium(IV) citrate replaced titanium(III) citrate under otherwise identical reaction conditions, no conversion to red1 occurred. Therefore, the reducing power of Ti(III) is required for the conversion. Conversion was less efficient when the reaction was performed at pH 7 (instead of pH 10.0) or at room temperature (instead of 60 °C). Treatment with dithionite results in the formation of the inactive MCR_{ox2} state, and redox mediators such as methyl viologen or triquat quench the ox1 signal and generate an EPR-silent and inactive form of the enzyme. The latter result makes electrochemical titrations of MCR a difficult challenge.

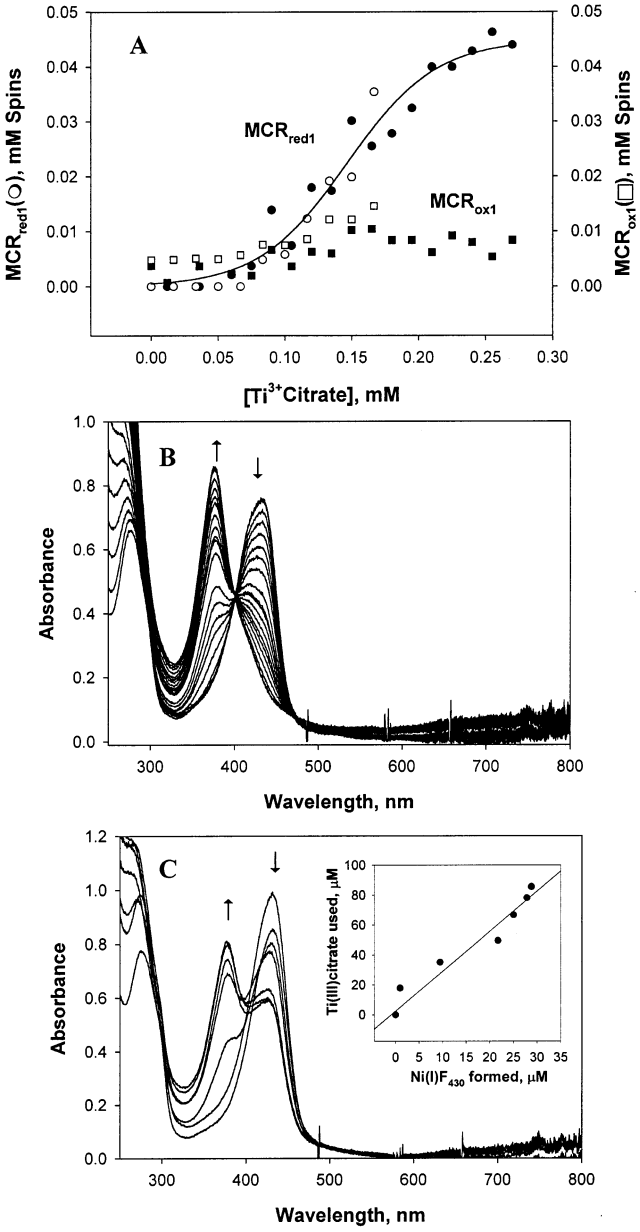

Figure 3. Redox titration of MCR and F_{430} with titanium(III) citrate. (A) Two independent experiments are overlaid. In each experiment, the conversion of 80 μM MCR_{ox1} (■, □; 0.49 spin/mol) to MCR_{red1} (○, ●) was measured. The slope at the midpoint ([titanium(III) citrate] = 0.147 ± 0.006 mM) of the curve was determined to be 2.9 (mM titanium(III) citrate)/(mM spins of MCR_{red1}). (B) Complete reduction of F_{430} was followed at pH 10.0 by UV−vis spectroscopy. The arrows indicate the decrease in the Ni(II) peak at 432 nm and the increase in the 376 nm band. (C) Titration of F_{430} at pH 7.6. Inset: Ti(III) oxidation associated with N(II) reduction. Ni(I)- and Ni(II)F430 were determined by UV−vis spectroscopy, while Ni(I) and Ti(III) were determined by EPR.

Although the results indicate that 3 electrons are associated with the conversion, there are several experimental problems associated with this experiment. One problem is that the ox1/red1 conversion requires either heating at 60 °C for 30 min or lengthy incubations (24 h at room temperature). These conditions

accelerate conversion of the Ni(I)-ox1 state to the Ni(II)-ox1 silent state (e.g., in the absence of Ti(III), all 80 μM ox1 is lost during the incubation, Figure 3A) and result in decay of Ti(III), even in our anaerobic chamber with O_2 levels below 1 ppm. Even at room temperature, there is significant disappearance of the Ti(III) EPR signal at pH 10.0. We attempted to determine how much Ti(III) is lost during the heating by performing a control titration with triquat (which has a low midpoint potential like MCR) replacing MCR; under the reaction conditions, free Ti(III) was not observed and the triquat EPR signal decayed, presumably because it underwent a second electron reduction or dimerization. Conversely, when excess Ti(III) is used during the titration of MCR, the EPR signal from Ti(III) remains after red1 has formed, indicating that Ti(III) binds and forms a relatively stable complex with MCR. Perhaps this is why Ti(III) is such an effective reductant, while dithionite, for example, is ineffective.

We also titrated coenzyme F_{430} with titanium(III) citrate, following the reduction by EPR (not shown) and by UV−vis spectroscopy at pH values of 10 (Figure 3B) and 7.6 (Figure 3C). During reduction, the UV−vis absorption peak at 432 nm associated with Ni(II)F_{430} shifts to 376 nm (see the arrows). Formation of the EPR-active Ni(I) state occurs simultaneously with the UV−vis spectral changes as shown earlier.[12] At pH 10.0 (Figure 3B), Ni(II)F_{430} is completely converted to the reduced Ni(I) state. However, at this pH, Ti(III) is unstable (see above) and is depleted even in the absence of F_{430}; thus, we could not accurately measure how much Ti(III) was oxidized during the reduction of F_{430}. However, at pH 7.6, Ti(III) is stable during the titration, allowing accurate measurement of the amount of Ti(III) present after the F_{430} and Ti(III) have reached equilibrium, as indicated by stabilization of the UV−vis spectrum. Parallel samples were analyzed by UV−vis spectroscopy and frozen in EPR tubes in liquid nitrogen for analysis of Ni(I) and remaining Ti(III). This protocol enables accurate measurement of the concentrations of Ni(I)- and Ni(II)F_{430} by UV−vis spectroscopy and Ni(I) and Ti(III) by EPR spectroscopy. The reduction reaches ~60% completion at pH 7.6. A linear least-squares fit of the data (Figure 3C, inset) indicates that 2.7 μM electrons are depleted per 1 μM conversion of the Ni(II) species (with the 432 nm peak) to the Ni(I) complex exhibiting the 376 nm peak.

Thus, chemical reduction of Ni(II)F_{430} to the state showing a Ni(I) EPR spectrum requires ~3 electrons, strongly indicating that this is not simply a 1-electron metal-centered process. Because of the experimental problems associated with performing titrations of MCR at high temperatures and at pH 10.0, we can only be confident that conversion of the ox1 to the red1 state requires 1−3 electrons. This is consistent with the hypothesis that 2 electrons are required for the conversion because transfer of an odd number of electrons should convert the EPR-active ox1 state to an EPR-silent state. We continue to assess ways to accurately measure the number of electrons required for the ox1 to red1 conversion. One could consider performing an oxidative titration of red1; however, this results in an EPR-silent Ni(II) state, not ox1, providing no relevant information about the activation process.

B. XAS Studies. The Ni K-edge XANES spectra for samples of MCR_{silent}, $MCR_{ox1\text{-}silent}$, MCR_{ox1}, and MCR_{red1} are compared in Figure 4, and the analysis of these data is summarized in

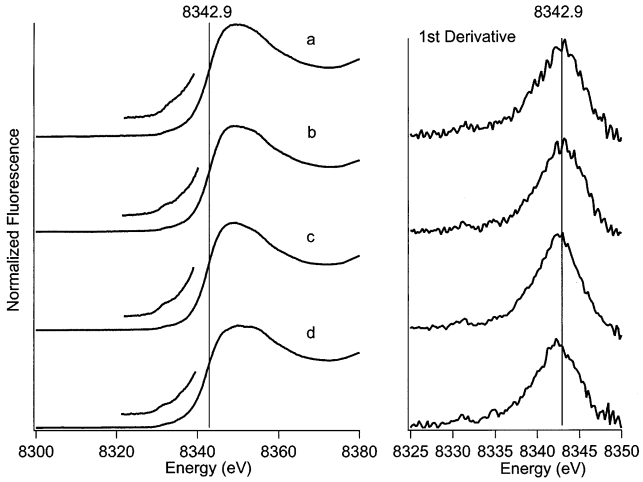

Figure 4. Left: XANES of (a) MCR_{silent}, (b) $MCR_{ox1\text{-}silent}$, (c) MCR_{ox1}, and (d) MCR_{red1} species from *M. marburgensis*. The inset plots are an expansion of the region around 8332 eV showing peaks assigned to 1s to 3d transitions. Right: First derivative of the XANES spectra. The center of the peak (first inflection point) is taken as the Ni K-edge energy (E_k) for each species. As a basis of comparison, the vertical line (8342.9 eV) indicates the Ni K-edge for the MCR_{silent} species.

Table 1. The redox activity of the Ni center is indicated by changes in the Ni K-edge energy, which varies systematically with the charge residing on the Ni center.[36] The edge energy, which is measured as the inflection point in the XANES spectra (determined as the maximum in the first-derivative spectrum) varies from 8342.9 eV in MCR_{silent} to 8342.4 eV in MCR_{red1}. This 0.5 eV range is about 25% of that expected from model studies for a 1-electron redox process centered on the Ni atom.[36] However, because the MCR_{ox1} and MCR_{red1} samples contain ~40% EPR-silent Ni (presumably the corresponding Ni(II) silent state), what is important are the trends, not the absolute numbers. It remains a goal to generate 100% EPR-active MCR; so far no one has generated above 0.8 spin/mol. Within experimental error, the observed energies fall into two groups: those of MCR_{silent} and $MCR_{ox1\text{-}silent}$ (Ni(II) states) are the same, as are those for MCR_{ox1} and MCR_{red1}. That the energies obtained from the MCR_{ox1} and MCR_{red1} states are 0.5 eV lower than those for the Ni(II) states indicates that the Ni centers in ox1 and red1 states are more electron-rich than in the silent states. This is consistent with both MCR_{ox1} and MCR_{red1} containing *formally* Ni(I) centers. Even if one "corrects" the data by using the edge energy obtained for the Ni(II) state present in the MCR_{ox1} and MCR_{red1} samples, the edge energy shifts observed for MCR_{ox1} are still no more than 50% of the ca. 2−3 eV shift expected for reduction of Ni(II) to Ni(I).[36] This indicates that the electron density changes associated with MCR activation are either modulated by the axial ligand environment or delocalized onto several atomic centers and not primarily localized on the Ni center.

Examination of preedge XANES for the MCR samples (Figure 4) does not reveal any peaks or shoulders corresponding to a $1s \rightarrow 4p_z$ electronic transition (with shakedown contributions) that are observed near 8338 eV in four-coordinate planar complexes or five-coordinate pyramidal complexes, including tetraazamacrocycles.[18,19,36] This rules out the presence of any four-coordinate planar F_{430} species in MCR_{silent}, $MCR_{ox1\text{-}silent}$, MCR_{ox1}, and MCR_{red1}. Analysis of the area under the preedge peak near 8332 eV that is assigned to a $1s \rightarrow 3d$ electronic

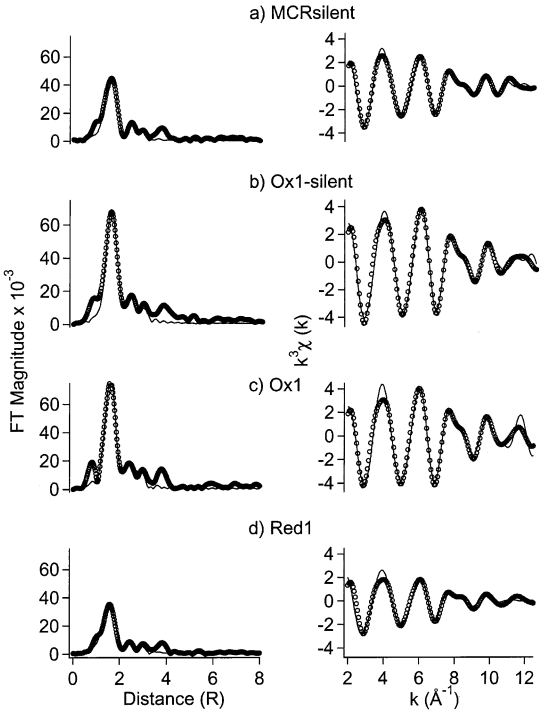

Figure 5. Fourier-transformed (left, $k = 2.0-12.5$ Å^{-1}) and Fourier-filtered (right, back-transform window, $r = 1.1-3.3$ Å, uncorrected for phase shifts) Ni K-edge EXAFS spectra from MCR samples (circles). The best fits (solid lines, from Table 2) to the data are as follows: (a) MCR_{silent}, fit 4; (b) $MCR_{ox1-silent}$, fit 7; (c) MCR_{ox1}, fit 5; (d) MCR_{red1}, fit 3. $MCR_{ox1-silent}$ (1.2 mM, EPR-silent but initially with 0.71 spin/mole in the ox1 state) was in 15% (v/v) glycerol, 50 mM Tris−HCl, pH 7.6. MCR_{ox1} (1.56 mM, with 0.8 spin/mol) was in 12% (v/v) glycerol, 50 mM Tris−HCl, pH 7.6. MCR_{silent} (1.35 mM) was in 15% (v/v) glycerol, 50 mM Tris−HCl, pH 7.6. MCR_{red1} (0.8 mM, 0.55 spin/mol, specific activity of 25 units/mg) was in 10% (v/v) glycerol, 0.6 M TAPS, pH 10, 3.5 mM titanium(III) citrate.

transition indicates that the values ($(1.6-3.2) \times 10^{-2}$ eV) all lie in the range appropriate for six-coordinate Ni centers (Table 1).[36] The range of areas for six-coordinate Ni 1s → 3d peaks is $(0.6-4.0) \times 10^{-2}$ eV, with a typical value of 2×10^{-2} eV. Five-coordinate complexes have an area ranging from 4.2×10^{-2} to 9.6×10^{-2} eV, with a typical value of 6×10^{-2} eV, and display a shoulder for the 1s → $4p_z$ transition in pyramidal complexes that is not observed for the MCR samples. Thus, the data are consistent with six-coordinate Ni centers in all of the MCR samples.

The EXAFS data and fits obtained for samples of MCR_{silent}, $MCR_{ox1-silent}$, MCR_{ox1}, and MCR_{red1} are compared in Figure 5. The amplitudes of the EXAFS features from the MCR_{silent} and MCR_{red1} data are much less intense than those from MCR_{ox1} and $MCR_{ox1-silent}$. This indicates that the ox1 and ox1-silent states contain either more scattering atoms or heavier atoms (e.g., S donors) than silent and red1, and/or that silent and red1 have a significantly more disordered primary coordination sphere. Calculated fits of the EXAFS spectra for MCR_{silent}, $MCR_{ox1-silent}$, MCR_{ox1}, and MCR_{red1} are summarized in Table 2. Three fits are shown for each sample: the fit generated using four first coordination sphere N atoms, the fit obtained when second coordination sphere C atoms from the F_{430} macrocycle are included, and the best fit obtained by adding axial ligands. The fits shown for MCR_{ox1} and MCR_{red1} were obtained from spectra of the samples containing ca. 40% EPR-silent species. However, the fits obtained from difference spectra do not vary significantly from the results shown (see the Supporting Information, Tables S2−S4). Because there is no reliable information regarding the EPR-silent species present in the samples, the uncorrected data are shown. The best fits have residuals of ca. 10%, indicating that the models fit the data extremely well out to a radial distance of ∼3.7 Å from the Ni. Fits using a single shell of N parameters always fit the data better than a single shell of S, indicating that the data are dominated by scattering from N/O donor atoms in all cases (not shown). This is expected because cofactor F_{430} contains four planar nitrogen ligands in the hydrocorphin ring system. Shells incorporating five or six N atoms gave better fits than those with four N atoms (not shown), another indication that one or two axial ligands are bound to the cofactor in each

Table 2. Summary of EXAFS Fits for MCR_{silent}, $MCR_{ox1-silent}$, MCR_{ox1}, and MCR_{red1}[a]

sample	no. of shells	N	r[b] (Å)	σ^2 (10^3 Å^{-2})	$\Delta\sigma^2$ (10^3 Å^{-2})	N_{frp}/N_{idp}	residual
			MCR_{silent}				
1	1	4	Ni−N = 2.089(1)	*10.1(1)*[c]	5.9	2/17	26.2
2	4	4	Ni−N = 2.087(1)	*10.1(1)*	5.9	6/17	11.3
		4	Ni−C = 3.026(1)	4.3(1)	−1.2		
		2	Ni−C = 3.430(1)	4.3(1)	−1.2		
		2	Ni−C = 3.265(1)	4.3(1)	−1.2		
3	5	4	Ni−N = 2.123(1)	*11.8(1)*	7.6	8/17	7.9
		4	Ni−C = 3.021(1)	7.4(1)	1.9		
		2	Ni−C = 3.011(2)	7.4(1)	1.9		
		2	Ni−C = 3.250(1)	7.4(1)	1.9		
		1	Ni−N = 2.014(1)	5.7(1)	1.1		
			$MCR_{ox1-silent}$				
1	1	4	Ni−N = 2.076(1)	6.0(1)	1.8	2/17	30.6
2	4	6	Ni−N = 2.078(1)	*10.2(1)*	6.0	6/17	11.3
		4	Ni−C = 3.055(2)	0.2(1)	−5.3		
		2	Ni−C = 2.911(1)	0.2(1)	−5.3		
		2	Ni−C = 3.199(1)	0.2(1)	−5.3		
3	6	4	Ni−N = 2.054(1)	6.4(1)	2.2	10/17	8.1
		4	Ni−C = 3.000(1)	2.3(1)	−3.2		
		2	Ni−C = 3.387(1)	2.3(1)	−3.2		
		2	Ni−C = 3.196(1)	2.3(1)	−3.2		
		1	Ni−S = 2.338(2)	7.4(1)	4.9		
		1	Ni−N = 2.277(2)	9.7(7)	5.1		
			MCR_{ox1}				
1	1	4	Ni−N = 2.075(1)	5.3(1)	1.1	2/17	32.1
2	4	4	Ni−N			6/17	no fit
		4	Ni−C				
		2	Ni−C				
		2	Ni−C				
2	5	4	Ni−N = 2.060(1)	4.9(1)	0.7	8/17	10.3
		4	Ni−C = 2.998(1)	2.1(1)	−3.4		
		2	Ni−C = 3.385(1)	2.1(1)	−3.4		
		2	Ni−C = 3.189(1)	2.1(1)	−3.4		
		1	Ni−S = 2.381(1)	5.9(1)	3.4		
			MCR_{red1}				
1	1	4	Ni−N = 2.075(1)	*13.9(1)*	9.7	2/17	25.5
2	4	4	Ni−N = 2.074(1)	*14.1(1)*	9.9	6/17	15.6
		4	Ni−C = 2.981(1)	*10.6(1)*	5.1		
		2	Ni−C = 3.007(1)	*10.6(1)*	5.1		
		2	Ni−C = 3.173(1)	*10.6(1)*	5.1		
3	5	4	Ni−N = 2.062(1)	*11.5(1)*	7.3	8/17	11.11
		4	Ni−C = 2.952(1)	9.0(1)	3.5		
		2	Ni−C = 3.010(1)	9.0(1)	3.5		
		2	Ni−C = 3.152(1)	9.0(1)	3.5		
		1	Ni−N = 2.252(1)	6.9(1)	2.3		

[a] σ^2 is the mean square disorder in the Ni−X distance, where X is the scattering atom, $\Delta\sigma^2$ is σ^2 relative to calculated values for reference compounds, and the residual (%) is the residual as defined in the Experimental Section. The accuracy of the distances determined by EXAFS for atoms in the first coordination sphere of the metal is limited to ±0.02 Å by the theoretical phase parameters. The refinements generally show precisions that are less than 0.02 Å for well-ordered shells; thus, differences in distances between samples using equivalent fits are more accurate than the absolute distances. [b] The distances shown are for the single-scattering pathways. [c] Italicized values are approaching physical insignificance. Large values of σ^2 suggest that the shell involved has a coordination number that is too large or is badly disordered and may be unnecessary for fitting the data.

Table 3. Summary of Ni Site Structural Parameters for MCR from XAS and Crystallographic Studies[a]

shell/state	silent		ox1-silent		ox1	red1
tetrapyrrole	EXAFS	crystal[b]	EXAFS	crystal[b]	EXAFS	EXAFS
4N	2.08(2)	2.08	2.05(2)	2.08	2.06(2)	2.06(2)
4C	3.03(5)		3.00(5)	2.98	3.00(5)	2.95(5)
2C	2.97(5)		3.20(5)	3.11	3.19(5)	3.01(5)
2C	3.25(5)		3.39(5)	3.22	3.39(5)	3.15(5)
av	3.06		3.15	3.07	3.14	3.02
			axial ligands			
bottom	N(O), 2.16(2)	O(Gln), 2.1	N(O), 2.28(2)	O(Gln), 2.1		N(O), 2.25(2)
top	N(O), 2.16(2)	$O(RSO_3^-)$, 2.1	1S, 2.34(2)	S(CoM), 2.4	1S, 2.39(2)	

[a] Distances in angstroms. [b] Ermler et al.[6]

of the four states. Separation of the first coordination sphere into two shells of scattering atoms did not significantly improve the residuals and often gave poorer fits than the best single-shell fit partly because the EXAFS data contain considerable intensity from second coordination sphere C atoms in the F_{430} macrocycle. Because data arising from the long axial ligand distances cannot be effectively separated from EXAFS arising from other atoms in either the first or second (macrocycle C atoms) coordination sphere by Fourier-filtering, it was necessary to develop a model that included the second coordination sphere C atoms.

The EXAFS from the second coordination sphere C atoms was modeled by three shells containing four, two, and two C atoms each (see the Experimental Section). Fits using a model for the macrocycle that includes the four first coordination sphere N atoms and the eight second coordination sphere C atoms gave large improvements in the fit (57%, MCR_{silent}; 63%, $MCR_{ox1\text{-}silent}$; 39%, MCR_{red1}) relative to a single shell of four N donor atoms (compare fits 1 and 2 for each sample in Table 2). To fit the data for $MCR_{ox1\text{-}silent}$, it was necessary to increase the number of first coordination sphere N atoms to six to account for additional EXAFS arising from first coordination sphere atoms. For MCR_{ox1}, no model lacking a S donor ligand could be refined (see the Supporting Information, Table S1). Inspection of the EXAFS features (compare Fourier-transformed spectra in Figure 5) arising from second and third coordination sphere atoms shows that the radial arrangement of atoms from the F_{430} macrocycle remains constant. The fits including second coordination sphere C atoms show little variation in either Ni−N or Ni−C vectors, showing that the macrocycle is maintained in a flat, equatorial arrangement about the Ni atom in all forms of MCR.

The results of refinements modeling the EXAFS arising from F_{430} in the samples were then used to obtain information regarding the axial ligands in each case. All five combinations of one or two O/N donor atoms (modeled with N parameters), one or two S donor atoms, or mixed O(N) + S donor atoms were examined for each sample (see the Supporting Information, Table S1). The best fits for the MCR_{silent} EXAFS data contain one or two additional O/N donors. The fit containing one O/N donor gave an axial Ni−O/N distance of 2.01 Å, which is shorter than those observed for the equatorial Ni−N bonds (MCR_{silent} fit 3, Table 2). This fit can be excluded because the XANES results show Ni is six-coordinate, and because the axial bond distance is unrealistic, particularly in view of the published crystal structure of this form of MCR.[6] The fit employing two axial O/N ligands gave a slight improvement in the residual over the fit with one axial ligand, and more reasonable axial Ni−O/N bond distances (2.16 Å, compared with 2.1 Å in the crystal structure, Table 3[6]), but has a very large value of σ^2 for that shell (see the Supporting Information, Table S1). This suggests that the bond lengths for the axial ligands are disordered in the sample, an observation that is consistent with the variability observed for these distances in various crystal structures.[6−8] The axial Ni−ligand distances observed in crystal structures are as follows: Ni−S, 2.40−2.53 Å; Ni−OSO_2−CoM, 2.29−2.32 Å; Ni−O_{Gln}, 2.08−2.36 Å. The best fit for $MCR_{ox1\text{-}silent}$ occurred with one S donor at 2.34(2) Å and one O/N donor at 2.28(2) Å (Table 2, $MCR_{ox1\text{-}silent}$ fit 3; a 28% improvement over $MCR_{ox1\text{-}silent}$ fit 2), distances that agree well with the range found in the relevant crystal structures (vide supra). No fit with only axial O/N donor ligands could be refined. ($MCR_{ox1\text{-}silent}$ fit 2 (Table 2) represents a fit with two N donors that were not refined separately from the F_{430} N donors.) For MCR_{ox1}, the best fit was obtained with one axial S donor at 2.38(2) Å (MCR_{ox1} fit 3, Table 2). The best fit for MCR_{red1} was with a single axial O/N donor ligand with a Ni−O/N distance of 2.25 Å (MCR_{red1} fit 3, Table 2; a 29% improvement over MCR_{red1} fit 2). A comparable, but inferior, fit that is consistent with the XANES results indicating that Ni is six-coordinate contains two axial O/N donors at an average distance of 2.23 Å (see the Supporting Information, Table S1). Again, the discrepancy presumably arises from disorder in the axial Ni−O/N distances.

The XANES and EXAFS results are consistent in indicating that all states contain a tetragonal Ni site with two elongated axial ligands. MCR_{silent} and MCR_{red1} appear to lack S donor ligation; however, the fits for $MCR_{ox1\text{-}silent}$ and MCR_{ox1} require one S donor ligand. The small changes in electron density indicated by the edge energy shifts, the lack of changes in geometry indicated by the XANES spectra, and the weak axial interactions implicit in the elongated axial ligands suggest that the macrocyclic ligand is intimately involved in the redox chemistry.

C. RR Studies. In the initial phase of the RR studies on MCR and isolated cofactor F_{430}, data were acquired using various exciting lines that accessed different regions of the broad, visible region, absorption profiles that are characteristic of the different states of the enzyme and the different oxidation states of the cofactor. The absorption spectra of cofactor F_{430} and MCR are shown in Figure 6 (left and right panels, respectively) with arrows indicating the various wavelengths used for the RR experiments. [We note that $MCR_{ox1\text{-}silent}$ (which was not examined by RR spectroscopy) exhibits an absorption spectrum similar to that of MCR_{silent}.] RR data sets were also acquired at different temperatures, which for MCR included 44, 150, 230, 277, and 298 K. The temperature profiles obtained for cofactor

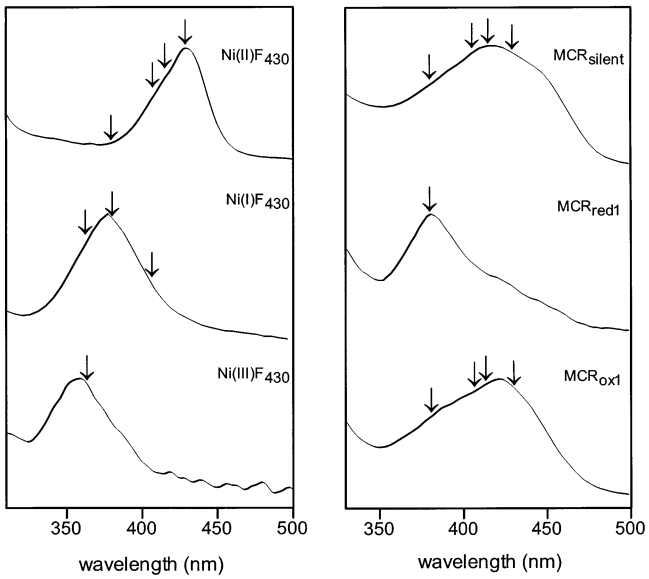

Figure 6. Absorption spectra of Ni(II), Ni(I), and Ni(III) cofactor F_{430} (left panel) and MCR_{silent}, MCR_{red1}, and MCR_{ox1} (right panel). The arrows indicate the various exciting lines used in the RR experiments. The spectra of the cofactor were obtained in the present study. The spectra of the enzyme were taken from ref 12. For MCR_{red1} and MCR_{ox1}, the spectra of the pure states were obtained by subtracting the spectrum of MCR_{silent} (see ref 12).

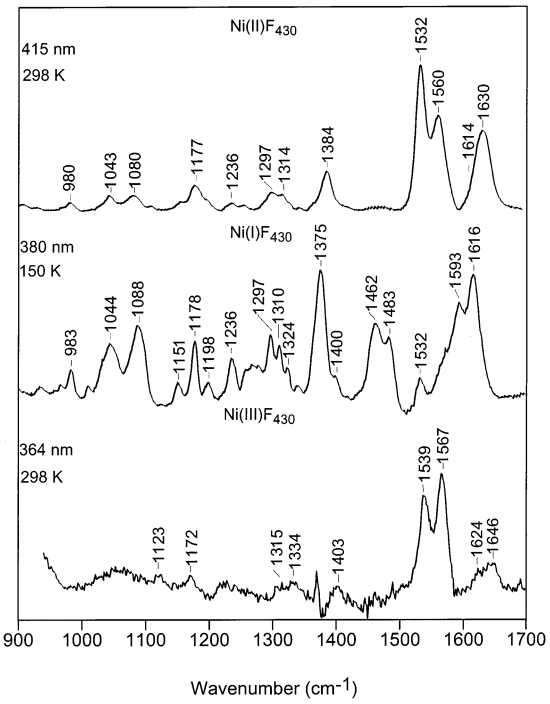

Figure 7. High-frequency RR spectra of Ni(II), Ni(I), and Ni(III) cofactor F_{430}. The excitation wavelength and temperature are indicated for each spectrum.

F_{430} were less extensive, but included both ambient and cryogenic regions (with the exception of Ni(III)F_{430}, which was examined only at ambient temperature). The purpose of these experiments was to determine whether significantly different RR features could be observed at the different excitation wavelengths and/or temperatures and to determine the optimum conditions for obtaining RR spectra. The ability to tune the excitation wavelength also permitted acquisition of RR spectra for MCR_{ox1} and MCR_{red1} that are free from interference from silent species, which are always present to some extent in the samples (the spin count for the RR samples typically ranged from 0.6 to 0.8). The salient observation of these experiments is that each of the species (Ni ion oxidation state of the cofactor or form of the enzyme) generally exhibits similar RR features at all measured excitation wavelengths and temperatures. The only spectral differences are in the relative intensities of certain RR bands. Accordingly, the RR spectra shown in the figures are generally representative of the different states of the cofactor and enzyme. The key features of these spectra are described in more detail below.

1. High-Frequency RR Spectra. a. Cofactor F_{430}. The high-frequency RR spectra of the Ni(II), Ni(I), and Ni(III) complexes of cofactor F_{430} are shown in Figure 7. Inspection of the RR data shows that the RR scattering characteristics of both the Ni(I) and Ni(III) complexes of cofactor F_{430} are very different from those of the Ni(II) complex and quite different from one another. The spectral differences among the different F_{430} complexes are the largest in the region above 1350 cm^{-1}. Accordingly, we will focus on this region of the RR spectra.

The RR spectrum of Ni(II)F_{430} is similar to that previously reported and includes bands at 1630, 1614, 1560, 1532, and 1384 cm^{-1}.[17,23−26] A number of other, generally weaker, bands are also observed. Previous RR studies have shown that Ni(II)F_{430} equilibrates between four- and six-coordinate complexes in aqueous medium in the absence of strong axial ligands. Under certain conditions, the six-coordinate complex can be exclusively formed.[17,23,26] Studies on the six-coordinate Ni(II)F_{430} have shown that the 1630, 1614−1560, and 1384 cm^{-1} bands are characteristic of this complex. The 1532 cm^{-1} band is the only unambiguous signature for the four-coordinate complex. Bands of the four-coordinate complex may also lie at frequencies similar to those observed for certain bands of the six-coordinate complex. However, this cannot be determined with certainty because the four-coordinate complex cannot be exclusively formed.

The RR spectrum of Ni(I)F_{430} in the 1350−1700 cm^{-1} region exhibits a pair of strong bands at 1616 and 1593 cm^{-1}, a second weaker pair of bands at 1483 and 1462 cm^{-1}, and a strong band at 1375 cm^{-1}. [The weak feature at 1532 cm^{-1} and the shoulder on the 1593 cm^{-1} band are due to a small amount of residual Ni(II) complex.] A reasonable assignment for the 1616 and 1593 cm^{-1} bands of Ni(I)F_{430} is that they are the downshifted analogues of the 1630 and 1614 cm^{-1} bands of six-coordinate Ni(II)F_{430}. Similarly, the 1375 cm^{-1} band of the former complex is the downshifted analogue of the 1384 cm^{-1} band of the latter. The correlation of either the 1483 or 1462 cm^{-1} band of the Ni(I)F_{430} complex with the 1560 cm^{-1} band of Ni(II)F_{430} seems unlikely. This correlation would require a downshift of 77 or 98 cm^{-1}, respectively. Frequency shifts of this magnitude upon changes in metal ion oxidation state in tetrapyrroles are unprecedented.[21,22] Accordingly, it seems more likely that the 1483 and 1462 cm^{-1} bands of Ni(I)F_{430} are new features that gain resonance enhancement only in the Ni(I) complex. This assignment further requires that the analogue of the 1560 cm^{-1} band of Ni(II)F_{430} is absent from the spectrum of the Ni(I) complex.

The RR spectrum of Ni(III)F_{430} in the 1350−1700 cm^{-1} region exhibits bands at 1646, 1624, 1567, 1539, and 1403 cm^{-1}. No bands are observed in the 1350−1390 cm^{-1} region (the feature in this region is a noise spike). A plausible correlation

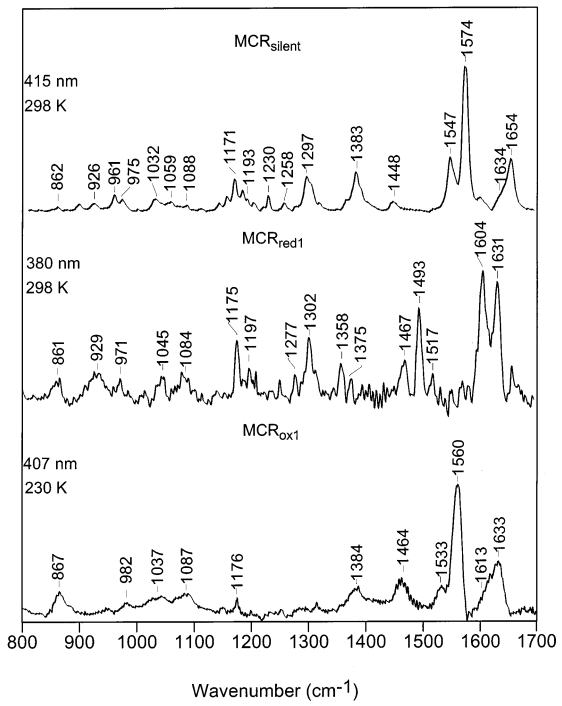

Figure 8. High-frequency RR spectra of MCR_{silent}, MCR_{red1}, and MCR_{ox1}. The excitation wavelength and temperature are indicated for each spectrum.

between the spectra of Ni(III) and Ni(II)F_{430} is that the 1646, 1624, 1567, 1539, and 1403 cm[1] bands of the former complex are the upshifted analogues of the 1630, 1614, 1560, 1532, and 1384 cm^{-1} bands of the latter. The correlation of the 1539 cm^{-1} band of Ni(III)F_{430} with the 1532 cm^{-1} band of Ni(II)F_{430} (which is due to the four-coordinate complex) would then indicate that the Ni(III)F_{430} exists in both four- and six-coordinate forms in solution. Regardless, a key observation is that oxidation of the nickel ion in cofactor F_{430} generally *upshifts* the highest frequency Raman bands, whereas reduction *downshifts* these bands.

b. MCR. The high-frequency RR spectra of MCR_{silent}, MCR_{red1}, and MCR_{ox1} are shown in Figure 8. Inspection of the RR data shows that the spectra of both MCR_{red1} and MCR_{ox1} are different from that of MCR_{silent} and notably different from one another. As is the case for the isolated cofactor, the spectral differences among the different forms of the enzyme are largest in the region above 1350 cm^{-1}. Accordingly, we will again focus on this region of the spectrum.

The spectrum of MCR_{silent} in the 1350−1700 cm^{-1} region is essentially identical to that previously reported.[25,26] Notable features in this spectrum include bands at 1654, 1634, 1574, 1547, and 1383 cm^{-1}. An important observation is that the RR spectrum of MCR_{silent} is different from that of six-coordinate Ni(II)F_{430}, despite the fact that the enzyme contains a six-coordinate cofactor. The spectral differences are manifested both in the frequencies of analogous RR bands and in the relative resonance enhancement of the RR bands. In general, the highest frequency RR bands of MCR_{silent} occur at higher frequencies than those of six-coordinate Ni(II)F_{430}. In particular, MCR_{silent} exhibits bands at 1654, 1634, and 1574 cm^{-1}, which are the analogues of the 1630, 1614, and 1560 cm^{-1} bands of six-coordinate Ni(II)F_{430}. The 1547 cm^{-1} band of MCR_{silent} is a new feature that is not observed in the RR spectrum of six-coordinate Ni(II)F_{430}. Recall that the 1532 cm^{-1} band of the isolated cofactor is not the analogue of the 1547 cm^{-1} band of MCR_{silent}, but rather is due to four-coordinate Ni(II)F_{430}. Only the 1384 cm^{-1} band of MCR_{silent} is at a frequency similar to that of its analogue in six-coordinate Ni(II)F_{430}. The RR spectral differences between MCR_{silent} and six-coordinate Ni(II)F_{430} have been previously noted and attributed to different conformations of the F_{430} macrocycle in the enzyme versus solution, despite the similar coordination numbers.[26] Regardless, the exact nature of these differences is not certain because X-ray crystallographic data are not available for the native form of the isolated cofactor.

The RR spectrum of MCR_{red1} in the 1350−1700 cm^{-1} region exhibits a pair of strong bands at 1631 and 1604 cm^{-1}, another pair of moderately intense bands at 1493 and 1467 cm^{-1}, and a third pair of weaker bands at 1375 and 1358 cm^{-1}. Comparison of the RR spectrum of MCR_{red1} with that of Ni(I)F_{430} (cf. Figures 7 and 8, second traces) reveals a number of striking similarities. The spectral pattern observed for the 1631, 1604, 1493, and 1467 cm^{-1} bands of MCR_{red1} is particularly close to that observed for the 1616, 1593, 1483, and 1462 cm^{-1} bands of Ni(I)F_{430}. Both MCR_{red1} and Ni(I)F_{430} exhibit a band at 1375 cm^{-1}. This band of the enzyme is much weaker than in the isolated cofactor. However, MCR_{red1} also exhibits a band at 1358 cm^{-1}, which is absent for Ni(I)F_{430}. Quite plausibly, this band is also present in the spectrum of the cofactor and overlaps the 1375 cm^{-1} band, thereby augmenting the intensity of this feature. In general, the spectra of MCR_{red1} and Ni(I)F_{430} are more similar to one another than are those of MCR_{silent} and six-coordinate Ni(II)F_{430}. The principal difference between the RR features of MCR_{red1} and Ni(I)F_{430} is that the four highest frequency bands of the enzyme are at higher frequencies than those of the cofactor. This trend is similar to that observed for MCR_{silent} versus six-coordinate Ni(II)F_{430}. Likewise, the single band that is at the same frequency in MCR_{red1} and Ni(I)F_{430} (∼1375 cm^{-1}) is also at the same frequency in MCR_{silent} and Ni(II)F_{430} (∼1384 cm^{-1}). Collectively, the RR data for the enzyme, in conjunction with those of the isolated cofactor, suggest that the conformational differences that exist between the cofactor in the enzyme versus solution persist upon reduction of the nickel ion (as evidenced by the systematic downshifts of the RR bands for cofactor F_{430} in solution versus the enzyme in both the Ni(I) and Ni(II) forms).

The RR spectrum of MCR_{ox1} in the 1350−1700 cm^{-1} region exhibits a pair of bands at 1633 and ∼1613 cm^{-1}, a second pair of bands at 1560 and 1533 cm^{-1}, a broad feature near 1464 cm^{-1}, and a weak band at 1384 cm^{-1}. The frequencies of the 1633 and 1613 cm^{-1} bands of MCR_{ox1} are qualitatively similar to those of the highest frequency pair of bands observed for MCR_{red1}. On the other hand, the relative intensities of the 1633 and 1613 cm^{-1} bands of MCR_{ox1} are quite different from those of the analogous pair of bands of MCR_{red1} and are more similar to the intensities of the 1654 and 1634 cm^{-1} bands of MCR_{silent}. The general appearance of the RR spectrum of MCR_{ox1} in the 1350−1600 cm^{-1} region is also quite different from that of MCR_{red1}. In particular, the 1560 and 1533 cm^{-1} bands of MCR_{ox1} appear to be moderately downshifted (∼14 cm^{-1}) analogues of the 1574 and 1547 cm^{-1} bands of MCR_{silent}. The 1383 cm^{-1} band appears to be the analogue of the band observed at a similar frequency for MCR_{silent}. The only other similarity in the spectra of MCR_{ox1} and MCR_{red1} is that both exhibit a band near 1465 cm^{-1} that is absent in the spectrum of MCR_{silent}.

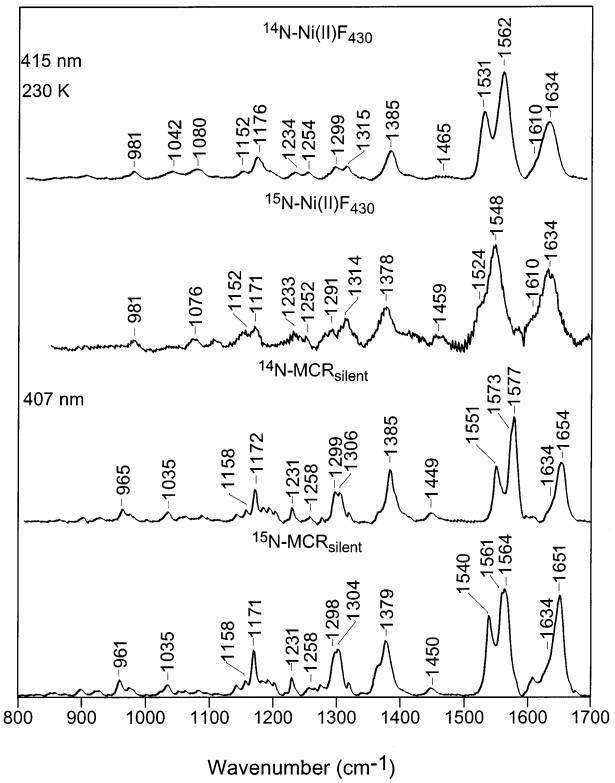

Figure 9. High-frequency RR spectra of ^{15}N-labeled Ni(II)F$_{430}$ in solution and in MCR$_{silent}$.

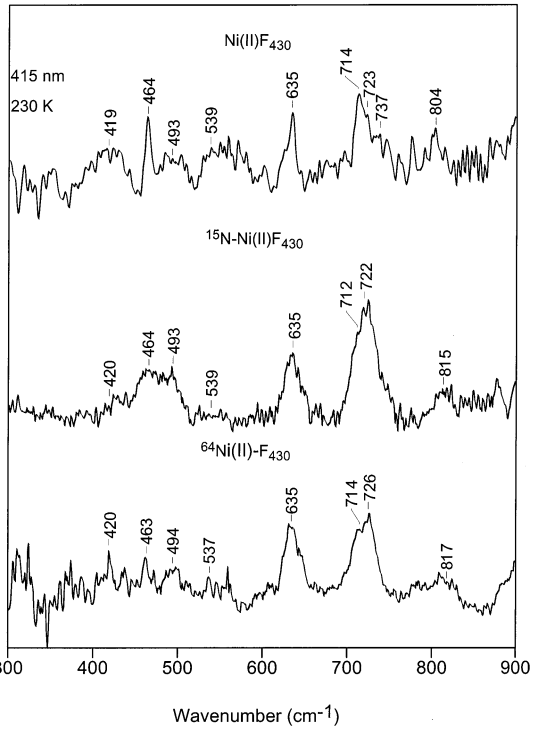

Figure 10. Low-frequency RR spectra of ^{15}N- and ^{64}Ni-labeled Ni(II)-F$_{430}$.

Collectively, the RR data for MCR$_{ox1}$ indicate that, despite the fact that this form of the enzyme contains Ni(I)F$_{430}$, the structure/conformation/axial ligation of the cofactor must be quite different from that in MCR$_{red1}$.

c. Isotope Studies. RR studies of the isotopically labeled cofactor were undertaken primarily with the objective of identifying the modes involving motions of the Ni−N$_{macrocycle}$ core and determining how the frequencies of these modes differ in the various forms of the enzyme. Accordingly, the studies of the isotopomers were directed primarily at the low-frequency region of the spectra. These results are described below. Nevertheless, the high-frequency RR spectra of the isotopomers provide insights into the composition of the normal modes of the F$_{430}$ macrocycle.

The high-frequency RR spectra of ^{15}N-labeled Ni(II)F$_{430}$ and MCR$_{silent}$ are compared with those of the normal isotopomer in Figure 9. The high-frequency spectra of the ^{64}Ni-labeled cofactor were also obtained, but are not shown because no spectral shifts are observed in this frequency region (as expected). Inspection of the data reveals that the two highest frequency modes (frozen solution, 1634 and 1610 cm^{-1}; enzyme, 1654 and 1534 cm^{-1}) are not (significantly) shifted in the ^{15}N isotopomer. Accordingly, these modes must be primarily due to stretching of the unsaturated C═C bridges between rings C and D and/or ring C and the exocyclic ring. [The carbonyl stretching mode of the exocylic ring would also be unaffected by ^{15}N substitution; however, this mode, which is expected in the 1680−1720 cm^{-1} region, is not observed in the RR spectrum.] In contrast, all of the other high-frequency modes are shifted upon ^{15}N labeling. For six-coordinate Ni(II)F$_{430}$, the 1562 and 1385 cm^{-1} bands are downshifted to 1548 and 1378 cm^{-1}, respectively. For four-coordinate Ni(II)F$_{430}$, the 1531 cm^{-1} band is downshifted to 1524 cm^{-1}. For MCR$_{silent}$, the 1577, 1551, and 1385 cm^{-1} bands are downshifted to 1564, 1540, and 1379 cm^{-1}, respectively. These shifts indicate that these modes contain significant C═N stretching character.

2. Low-Frequency RR Spectra. As noted above, the objective of the low-frequency RR studies was to identify modes that involve motions of the Ni−N$_{macrocycle}$. Presumably, certain of these modes, if they could be identified, would also be sensitive to axial ligation of the nickel ion. The low-frequency RR studies focused on Ni(II)F$_{430}$, MCR$_{silent}$, and MCR$_{ox1}$. The low-frequency spectra of Ni(I)F$_{430}$ and MCR$_{red1}$ were also examined; however, these samples exhibited very poor RR scattering characteristics and were not pursued past initial screening.

The low-frequency RR spectra of Ni(II)F$_{430}$ and the ^{15}N and ^{64}Ni isotopomers are shown in Figure 10. The analogous spectra for MCR$_{silent}$ are shown in Figure 11. The spectral quality for the enzyme is generally superior to that for the cofactor. Both the cofactor and enzyme exhibit a number of low-frequency modes. However, the RR bands in the lowest frequency region (below 500 cm^{-1}), where Ni−N$_{macrocycle}$ and or Ni−axial ligand stretches would be expected, are extremely weak. This was also the case for MCR$_{ox1}$ (not shown). On the basis of the low-frequency RR data, we are unable to identify any bands that exhibit significant shifts upon isotopic substitution, with the possible exception of the 397 and 338 cm^{-1} bands of MCR$_{silent}$. The 397 cm^{-1} band appears to downshift to 394 cm^{-1} in the ^{64}Ni isotopomer. The 338 cm^{-1} band appears to downshift in both the ^{15}N and ^{64}Ni isotopomers, to 335 and 331 cm^{-1}, respectively. On the basis of this observation, isotope difference spectra were carefully examined (not shown). The appearance of these spectra cast doubt on the authenticity of the shifts for these two modes. Instead, the shifts appear to be artifacts due to very weak features on nonlevel baselines. Collectively, the

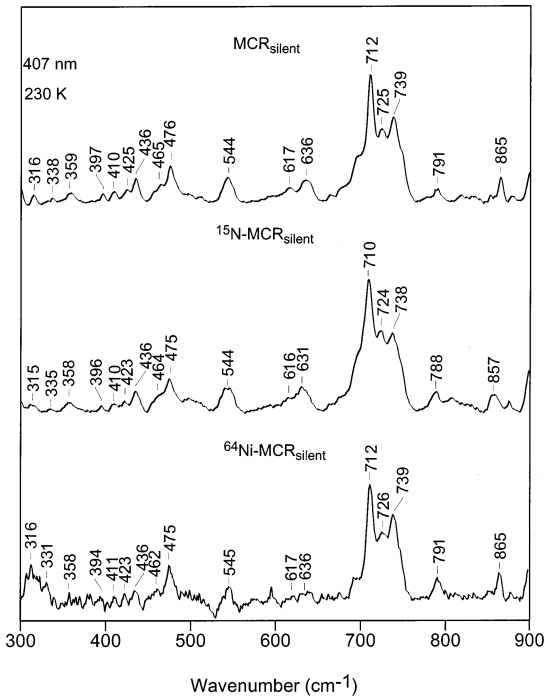

Figure 11. Low-frequency RR spectra of ^{15}N- and ^{64}Ni-labeled Ni(II)F_{430} in MCR_{silent}.

low-frequency RR data suggest that vibrations involving motions of the Ni−$N_{macrocycle}$ core of cofactor F_{430} are not appreciably resonance enhanced. The poor resonance enhancement of these modes further suggests that it would be unlikely that Ni−axial ligand modes would gain appreciable resonance enhancement. Thus, the best information obtained regarding axial ligation is from the XAS studies.

IV. Discussion

A. Oxidation and Ligation States of MCR_{ox1} and MCR_{red1} and Mechanism of Activation. Activation of MCR involves Ti(III)-dependent conversion of MCR_{ox1} to the MCR_{red1} state. Although titanium(III) citrate is not the physiological electron donor, it has been conclusively shown that this method generates catalytically active red1 and that the amount of active enzyme is related to the amount of red1 generated by this method.[11,12] The EPR spectrum of the enzyme generated by this method is identical to that of red1 generated by treating cells with H_2 before harvesting.[9] This indicates that the Ni coordination state is the same regardless of whether red1 is generated by H_2 or Ti(III). Although H_2 is the ultimate electron donor for the cells and presumably the physiological reductant, Ti(III) reproducibly generates higher yields of red1. Titanium(III) citrate is also the electron donor used in the standard assay of MCR. Therefore, we conclude that changes in MCR that accompany the Ti(III)-dependent activation are physiologically and mechanistically relevant.

Chemical reduction of Ni(II)F_{430} by titanium(III) citrate to an EPR-active Ni(I) state that exhibits a UV−vis absorption peak at 376 nm requires 3 electrons. Furthermore, Ti(III)-dependent reduction of the Ni(I)MCR_{ox1} to the Ni(I)MCR_{red1} state requires ~2 electrons. Ni(I)MCR_{ox1} and Ni(II)F_{430} exhibit similar UV−vis spectra, as do Ni(I)MCR_{red1} and Ni(I)F_{430}. These apparently paradoxical results are consistent and strongly indicate that these stable reduced Ni(I) species are not (only) reduced at the metal center. A 1-electron reduction of Ni(II)-F_{430} to Ni(I)F_{430} plus a 2-electron reduction of the corphin ring would explain the 3-electron reduction of the F_{430} pentaacid. Similarly, 2-electron reduction of the macrocycle would explain the conversion of Ni(I)MCR_{ox1} to Ni(I)MCR_{red1}. These results are in apparent contradiction with cyclic voltammetry experiments on the Ni(II) pentamethyl ester of F_{430} in organic solvents that clearly show a reversible 1-electron reduction.[45] However, it has not been possible to generate Ni(I)F_{430} via bulk electrolysis; a "stable" reduced species apparently can only be generated via chemical reduction (Na amalgam for the pentamethyl ester;[45] titanium(III) citrate for the pentaacid[32]). Because the Na amalgam reduction is uncontrolled, one cannot assess how many electrons are required to form the stable reduced species. In a previous study of the Ti(III)-dependent reduction of F_{430} pentaacid at pH 10.0, the data were fit to a 1-electron reduction.[32] However, we have reanalyzed these data and find that $n = 2$ fits far better. In summary, the redox titrations indicate that the stable reduced species of MCR and NiF_{430} that have been studied spectroscopically are more than 1-electron-reduced.

Because cofactor F_{430} can epimerize upon heating,[46] one might wonder whether the observed spectral changes might (at least in part) be due to formation of the diepimeric form of the coenzyme. However, both RR and XAS spectra indicate that the diepimer is not formed upon Ti(III)-dependent activation. The diepimer exists only as a four-coordinate form in solution, is highly nonplanar, and exhibits RR bands at much lower frequencies than those of the six-coordinate native form. The RR and XAS spectra of the enzyme show only the six-coordinate form, indicating that epimerization has not occurred.

The RR and XAS results are consistent with magnetic resonance experiments[13,14] that indicate that both the ox1 and red1 states contain the Ni(I) form of the cofactor. The X-ray absorption edge energies observed for the MCR_{ox1} and MCR_{red1} states are 0.5 eV lower than those for the Ni(II) states, indicating that the Ni centers in the ox1 and red1 states are more electron-rich than in the silent states. This characteristic is consistent with both MCR_{ox1} and MCR_{red1} containing formally Ni(I) centers. The RR results concur with this conclusion. In particular, the ox1 and red1 forms exhibit ring-skeletal modes that are downshifted relative to those of the Ni(II) silent form. This behavior is also consistent with that observed for reduction of the nickel ion in isolated cofactor F_{430} and inconsistent with the trends observed for oxidation (which generally *upshifts* the highest frequency ring-skeletal modes). Regardless, the substantial differences between the RR spectra of MCR_{ox1} and MCR_{red1} indicate that the structure/conformation/axial ligation of the cofactor in the two states must be quite different.

Reductive activation of MCR by titanium(III) citrate, which is accomplished by input of approximately 2 electrons, does not alter the redox state of nickel. Furthermore, XAS experiments indicate that both ox1 and red1 are six-coordinate. Presumably, the glutamine oxygen remains as the lower axial ligand in all the Ni(II) and Ni(I) states. Thus, from a "nickel-centric" view of MCR, the major difference between the ox1 and red1 states is that ox1 contains an upper axial thiolate ligand, which is replaced by a nitrogen/oxygen ligand upon conversion

(45) Jaun, B.; Pfaltz, A. *J. Chem. Soc., Chem. Commun.* **1986**, 1327−1329.
(46) Pfaltz, A.; Livingston, D. A.; Jaun, B.; Diekert, G.; Thauer, R. K.; Eschenmoser, A. *Helv. Chim. Acta* **1985**, *68*, 1338−1358.

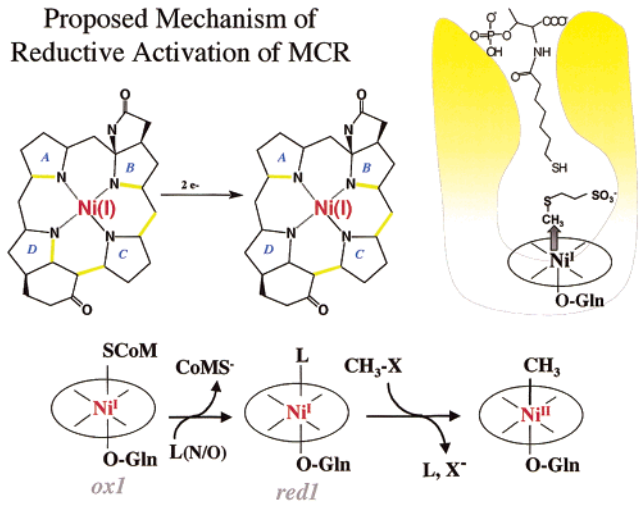

Figure 12. Schematic diagram of the activation of MCR_{ox1} to the MCR_{red1} state.

to the red1 state. Because crystallographic studies of $MCR_{ox1\text{-}silent}$ reveal coordination of the thiolate of CoM to the upper axial site,[6] we presume that the thiolate observed in the XAS spectra of MCR_{ox1} also is derived from CoM. This conclusion is supported by cryoreduction experiments in which γ-irradiation of $MCR_{ox1\text{-}silent}$ at 77 K directly yields a significant amount of MCR_{ox1}.[13] Treatment with titanium(III) citrate clearly results in a ligand switch. What then is the upper ligand in the red1 state, which contains two oxygen/nitrogen axial ligands? Because the crystal structure of the MCR_{silent} state shows the sulfonate oxygen of CoM ligated to nickel, perhaps this O donor ligand remains in the MCR_{red1} state. However, cryoreduction and other recent experiments indicate that, upon reduction, another oxo ligand replaces the sulfonate.[13] Cryoreduction at 77 K generates a form of the enzyme similar to red1, but with a significantly larger value of $g_{||}$. When the cryoreduced sample is warmed (annealed), this species is replaced by another with EPR and ENDOR parameters identical to those of MCR_{red1}.[13] Furthermore, the sulfonate-ligated form of MCR_{red1} has distinct spectroscopic parameters (Singh, Horng, and Ragsdale, manuscript in preparation). Therefore, as shown in Figure 12, reductive activation of MCR must involve replacement of the upper axial thiolate with a weak oxy or nitrogen ligand.

The net effect of the conversion of ox1 to red1 is to poise the enzyme for interaction with the methyl group of methyl-SCoM; however, the changes in ligation do not explain the requirement for a reductant (titanium(III) citrate). Furthermore, it is clear that the marked changes in the RR spectrum reflect much more significant structural alterations than switching one ligand. As was previously noted, the RR spectrum of MCR_{ox1} is qualitatively more similar to that of MCR_{silent} than is the spectrum of MCR_{red1}. The basis for this assessment is that the RR spectra of both MCR_{ox1} and MCR_{silent} exhibit a pair of bands in the 1530−1580 cm^{-1} region that are due to vibrations that contain substantial C═N stretching character, whereas these bands are absent in the spectrum of MCR_{red1}. The key question is what gives rise to these large vibrational differences. In this regard, XAS studies strongly suggest that both the ox1 and red1 states are six-coordinate Ni(I) forms. The only clearly delineated difference between the structures of MCR_{ox1} and MCR_{red1} is in the nature of the axial ligands. In particular, MCR_{ox1} has an upper axial thiolate ligand (from $CoMS^-$) and a lower axial oxygen donated by the side chain of Gln-α147. Treatment with titanium(III) citrate may promote removal of the upper axial thiolate ligand, producing MCR_{red1} with an upper coordination site that may be more labile with respect to substitution. It seems unlikely, however, that this ligand switch alone would be sufficient to explain the large differences in the core-mode vibrational characteristics of the red1 versus ox1 states.

Collectively, our results suggest that reductive activation elicits quite far-reaching effects on the structure of the hydrocorphin ring of cofactor F_{430}. The largest structural perturbations do not appear to involve the C═C double bonds of the ring, as is evidenced by the fact that the ^{15}N-insensitive skeletal vibrations of MCR_{silent} (1634/1650 cm^{-1}) have analogues in both MCR_{red1} (1604/1631 cm^{-1}) and MCR_{ox1} (1613/1633 cm^{-1}). On the other hand, certain C═N bonds of the hydrocorphin ring appear to be strongly perturbed in MCR_{red1} relative to either MCR_{ox1} or MCR_{silent}. This is evidenced by the fact that the RR spectrum of MCR_{red1} (and isolated $Ni(I)F_{430}$) does not exhibit clear analogues for two ^{15}N-sensitive skeletal modes that are observed for both MCR_{ox1} (1533/1560 cm^{-1}) and MCR_{silent} (1547/1574 cm^{-1}). The fact that reductive activation strongly affects two vibrations that contain significant C═N stretching character further suggests that the structural perturbation of the hydrocorphin ring occurs in either ring B or ring D (rather than ring A or C; see below). One plausible explanation for the perturbation of the imino bonds of rings B and D in MCR_{red1} is that one of these rings has undergone a 2-electron reduction. The net effect of this reduction would be to decrease the conjugation of the cofactor by one double bond. If the reduction occurs at ring D, it would also remove the carbonyl group in the fused ring from conjugation. However, we have not identified this vibration in the RR spectra of any states of the cofactor (enzyme-bound or in solution), indicating that this bond is not strongly conjugated to the extended network within the ring, even in the MCR_{silent} and MCR_{ox1} states.

In a resonance form of the F_{430} structure shown in Figure 1, four double bonds among rings B, C, and D are conjugated, while the double bond in ring A is isolated. Reduction of a double bond in ring B or D (at the end of the network of conjugation) would result in a clear change in the UV−vis spectrum of the cofactor. Consistent with this view, the absorption maximum of MCR_{red1} (and $Ni(I)F_{430}$) is blue shifted by nearly 40 nm relative to that of MCR_{ox1} (see Figure 6). This was previously a puzzling characteristic of the absorption spectrum that is explained by our hypothesis that the cofactor has undergone a net 2-electron reduction because removal of a terminal double bond of any extended conjugated system results in approximately a 40 nm blue shift. This hypothesis also explains another perplexing aspect of the titanium(III) citrate-dependent reductive activation of MCR. In particular, approximately 2 electrons from this low-potential reductant are required to convert the Ni(I)-ox1 state of the enzyme to the Ni(I)-red1 form. Furthermore, sodium borohydride, which is a 2-electron reductant that is commonly used to reduce C═N bonds, can convert MCR_{ox1} to MCR_{red1} (Horng and Ragsdale, unpublished data).

The assessment that a 2-electron reduction of the macrocycle must occur in either ring B or ring D rather than ring A or C is supported by the following considerations: (1) Reduction of

ring A would affect only a single C═N stretching vibration (rather than the multiple vibrations observed) because this bond is isolated from the π-conjugation network of the macrocycle. This isolation effectively decouples the C═N stretching mode of ring A from those of rings B and D (and C). It should also be noted that the isolation of ring A from the π-conjugation network would preclude resonance enhancement of the C═N stretching vibration of this ring because the absorption associated with this C═N bond would fall in the vacuum UV region. (2) Reduction of ring C would break the π-conjugation network into two isolated, smaller π-conjugation networks. Each of these two smaller π-conjugated systems would absorb much further into the UV region than is observed for MCR_{red1}.

One might speculate about what poises MCR_{ox1} in particular toward reductive activation. Perhaps the upper axial thiolate ligand at the base of a highly protected cavity in the protein, with its propensity to delocalize electron density into the metal center, is uniquely qualified to direct the electrons to the terminal bond of the extended π-network. In solution, the cofactor is freely accessible and would not require the participation of the thiolate. One might also speculate that the macrocycle participates in catalysis. If the reduction of the macrocycle is reversible, the 2 electrons from the ring could be directed to the methyl group during the formation of methane. In this regard, we have no evidence for a 30 nm red shift during transient kinetic analysis of methane formation, which indicates that ring reduction is only necessary for activation of the enzyme, not catalysis, or that the oxidized ring is a transient intermediate that is rapidly rereduced to the MCR_{red1} state.

B. Catalytic Mechanism. Two aspects of MCR_{red1} may be important for catalysis. The additional 2 electrons in the ring might allow greater flexibility of cofactor F_{430} and could even serve as a transient source of 2 electrons for the 2-electron reduction of methyl-SCoM to methane. Furthermore, the upper axial "oxo/nitrogen" Ni(I) ligand may be relatively exchange labile, which would poise the Ni ion for interaction with the methyl group and for formation of the proposed methyl-Ni intermediate. Preliminary results indicate this to be the case (Singh, Horng, and Ragsdale, manuscript in preparation). There are several possible mechanisms by which this intermediate could be formed. A dissociative transition state in which the upper axial ligand is removed before Ni(I) and the methyl group interact is feasible. Recent work by Meyerstein suggests the possibility of an associative mechanism in which the upper axial oxo/nitrogen ligand remains as the methyl-Ni bond is formed.[47−49] In the latter scenario, methyl transfer could be viewed as a ligand-exchange reaction.

V. Conclusions

The results described herein strongly indicate that activation of the ready ox1 state to the active red1 state of MCR involves a ligand switch (thiolate to oxo or nitrogen) and 2-electron reduction of the macrocyclic nickel ligand, but no redox changes at the metal center. Furthermore, this reduction is paralleled in cofactor F_{430} in solution. Indeed, the RR spectra of $Ni(I)F_{430}$ are more similar to those of MCR_{red1} than those of MCR_{ox1}. MCR_{ox1} is catalytically inactive, but apparently is the only form of MCR that can undergo conversion to the red1 state. The unexpected results and the conclusions described here suggest a number of experiments to further test the hypothesis that macrocyclic ring reduction is key to the activation of MCR.

Acknowledgment. This work was supported by Grant GM-36243 from the National Institute of General Medical Sciences (D.F.B.) and Grant ER-20053 from the Department of Energy (S.W.R.). The NSLS at Brookhaven National Laboratory is supported by the U.S. Department of Energy, Division of Materials Sciences and Division of Chemical Sciences. Beamline X9B at the NSLS is supported in part by NIH Grant RR-01633. We thank Drs. D. F. Becker and K. Czarnecki for contributing to the initial RR studies and Dr. J. R. Diers for assisting with the electrochemical measurements.

Supporting Information Available: Tables containing a summary of EXAFS fits for MCR_{silent}, $MCR_{ox1\text{-}silent}$, MCR_{ox1}, and MCR_{red1}, a summary of EXAFS fits for MCR_{ox1} − 37% $MCR_{ox1\text{-}silent}$, a summary of EXAFS fits for MCR_{ox1} − 37% MCR_{silent}, and a summary of EXAFS fits for MCR_{red1} − 35% MCR_{silent} (PDF). This material is available free of charge via the Internet at http://pubs.acs.org.

JA020314H

(47) Goldstein, S.; Czapski, G.; van Eldik, R.; Shaham, N.; Cohen, H.; Meyerstein, D. *Inorg. Chem.* **2001**, *40*, 4966−4970.
(48) Van Eldik, R.; Meyerstein, D. *Acc. Chem. Res.* **2000**, *33*, 207−214.
(49) Shaham, N.; Cohen, H.; van Eldik, R.; Meyerstein, D. *J. Chem. Soc., Dalton* **2000**, 3356−3359.